



รายงานวิจัยฉบับสมบูรณ์

โครงการ การประเมินความปลอดภัยของโครงสร้างโดยระเบียบวิธี พลาสติกสเกลบาวดารีไฟในต์เอเลเมนต์

โดย รองศาสตราจารย์ ดร. เสวกชัย ตั้งอร่ามวงศ์ และคณะ

รายงานวิจัยฉบับสมบูรณ์

โครงการ การประเมินความปลอดภัยของโครงสร้างโดยระเบียบวิธี พลาสติกสเกลบาวดารีไฟในต์เอเลเมนต์

รศ.ดร. เสวกชัย ตั้งอร่ามวงศ์

คณะวิศวกรรมศาสตร์ จุฬาลงกรณ์มหาวิทยาลัย

สนับสนุนโดยสำนักงานกองทุนสนับสนุนการวิจัยและจุฬาลงกรณ์ มหาวิยาลัย (ความเห็นในรายงานนี้เป็นของผู้วิจัย สกว.และต้นสังกัดไม่จำเป็นต้องเห็นด้วยเสมอไป)

i

กิตติกรรมประกาศ

โครงการวิจัยนี้ได้รับทุนพัฒนานักวิจัยรุ่นกลาง ประจำปีงบประมาณ พ.ศ. 2562 ภายใต้สัญญาเลขที่ RSA6280089 คณะผู้วิจัยขอขอบพระคุณเป็นอย่างยิ่ง และขอขอบคุณจุฬาลงกรณ์มหาวิทยาลัย และคณะ วิศวกรรมศาสตร์ ที่ให้ความอนุเคราะห์ในการทำวิจัย

รศ. ดร. เสวกชัย ตั้งอร่ามวงศ์

31 ตุลาคม 2565

สารบัญ

กิตติกรรมประกาศ	i
สารบัญ	ii
สารบัญภาพ	iv
สารบัญตาราง	vi
บทคัดย่อ	vii
เนื้อหางานวิจัย	1
1. วัตถุประสงค์	1
2. วิธีทดลอง	3
2.1 Scaled Boundary Finite Element Framework	3
Generic SBFE model and formulations	3
Quadtree model construction of in-plane structural system	7
Collapse load determination by iterative elastic SBFE analyses	10
2.2 Node-Based Finite Element Framework	14
Generic three-node NS-FE model and formulations	14
Automatic adaptive NS-FE seheme	17
Collapse load determination by iterative elastic NS-FE analyses	19
2.3 Edge-Smoothed Finite Element Framework	24
Generic ES-FEM model and formulations	24
Recovery stress field	27
Automatic adaptive ES-FE approach	27
Collapse load determination by iterative elastic ES-FE analyses	29

3.	ผลการทดลอง	. 30
	3.1 Double-Edge Notch Specimen	. 30
	3.2 Collapse load determination by iterative elastic SBFE analyses	. 31
	3.3 Collapse load determination by iterative elastic NS-FE analyses	. 34
	3.4 Collapse load determination by iterative elastic ES-FE analyses	. 41
4.	สรุปและวิจารณ์ผลการทดลอง	. 45
เอกสา	รอ้างอิง	. 48
ผลลัพ	ธ์ที่ได้จากโครงการ	. 52
ผล	งงานตีพิมพ์ในวารสารวิชาการนานาชาติ	. 52
กา	รนำผลงานวิจัยไปใช้ประโยชน์	. 52
อื่เ	រុទ្	. 53

สารบัญภาพ

Figure 1. Generic SBFE subdomain (a) 2D case, (b) 3D case	4
Figure 2. Flowchart for quadtree mesh generation procedures	8
Figure 3. Signed distance function of a point inside the domain (X_1) , on the boundary (X_2)), and
outside the domain (X ₃ and X ₄)	9
Figure 4. Square plate with circular hole (a) geometry, (b) initial quadtree grid mesh	10
Figure 5. SBFE meshes around circular hole (a) standard polygon subdomains, (b) qua	ıdtree
refinement	10
Figure 6. Generic three-node NS-FE model with smoothing (shaded) domains	14
Figure 7. Newest bisection adaptive (refining and coarsening) mesh scheme	18
Figure 8. Generic three-node ES-FE model with smoothing (shaded) domains	24
Figure 9. Adaptive mesh (refining and coarsening) construction	28
Figure 10. Double-edge notch specimen	31
Figure 11. Schematic SBFE model.	31
Figure 12. Iterative elastic SBFE analysis solutions (a) $lpha'/\sigma_{\!\scriptscriptstyle 0}$ – i responses, (b) von Mises	stress
distribution at $\mathbf{Q}^{\mathrm{col}}/oldsymbol{\sigma}_{\!\scriptscriptstyle{\mathrm{o}}}$	32
Figure 13. Iterative $lpha^i/\sigma_{\!\scriptscriptstyle 0}$ – i responses for various values of λ	33
Figure 14. Various schematic NS-FE models of a quarter of double-edge notched specim	en (a)
crisscross-, (b) slash- and (c) distorted mesh pattern (δ = 0.5)	35
Figure 15. $oldsymbol{lpha}$ col solutions for various crisscross-mesh models	35
Figure 16. $oldsymbol{lpha}$ col solutions for various slash-mesh models	36
Figure 17. Deformations at plastic collapse for various uniform slash-mesh models	36
Figure 18. $lpha$ col solutions for various distorted and slash-shaped NS-FE models	37
Figure 19. Monotonically incremental $lpha$ i responses of a non-uniform NS-FE model	with
Nm = 1370.	39

Figure 20. Collapse mechanisms for various non-uniform NS-FE models (a) deformations, (b)
modified modulus distributions
Figure 21. Double-edge notched specimen (a) geometry and loading, (b) schematic discrete
model (Nm = 16), where solid lines indicate restrained boundary conditions
Figure 22. Double-edge notched specimen: load multiplier responses $lpha$ i by RES-FEM, ES-FEM
and FEM (Nm = 8192)
Figure 23. Double-edge notched specimen: collapse load solutions $lpha$ col for various degrees
of freedom Nd
Figure 24. Double-edge notched specimen: progressive adaptive meshes of RES-FEM at $lpha$ col.
44
Figure 25. Double-edge notched specimen: modified modulus distributions by adaptive RES-
FEM (Nm = 2952) at various iterations i

สารบัญตาราง

Table 1. Double-edge notch specimen model and $lpha^{ m col}/\sigma_{\!\! o}$ solutions for different structural
discretization
Table 2. α^{col} solutions of von Mises notched specimen ($\alpha^{co,refl}$ = 1.1316) by uniform and
automatic adaptive NS-FEMs
Table 3. α^{col} solutions of von Mises notched specimen ($\alpha^{col,ref}$ = 1.1316) by various analysis
methods
Table 4. Double-edge notched specimen: collapse load solutions $oldsymbol{lpha}^{ ext{col}}$ by various RES-FEM
solves
Table 5. Double-edge notched specimen: collapse load solutions $lpha$ col by various analysis
methods43

บทคัดย่อ

รหัสโครงการ: RSA620089

ชื่อโครงการ : การประเมินความปลอดภัยของโครงสร้างโดยระเบียบวิธีพลาสติกสเกลบาวดารีไฟในต์เอเลเมนต์

ชื่อนักวิจัย : รศ.ดร. เสวกชัย ตั้งอร่ามวงศ์ คณะวิศวกรรมศาสาตร์ จุฬาลงกรณ์มหาวิทยาลัย

อีเมลล์ : sawekchai.t@chula.ac.th

ระยะเวลาโครงการ : 3 ปี

เพื่อยืดอายุการใช้งานของโครงสร้างพื้นฐานต่างๆ ได้อย่างยั่งยืน

โครงงานวิจัยนี้นำเสนอการพัฒนาเทคโนโลยีนวตกรรมของการสร้างแบบจำลองและเครื่องมือเชิงตัวเลขสำหรับ การประเมินความปลอดภัยของโครงสร้างอย่างมีประสิทธิภาพ ในขณะที่เทคนิคการวิเคราะห์และออกแบบ ส่วนมากมีแนวโน้มที่จะพบอุปสรรค์จากความต้องการการวิเคราะห์อย่างเข้มข้นถึงรูปแบบวิวัฒนาการของ พฤติกรรมอย่างสมบูรณ์ของโครงสร้าง 3 มิติ ขนาดใหญ่ ระเบียบวิธีที่ถูกนำเสนอนี้จึงขยายขอบเขตของวิธีการ วิเคราะห์แบบพลาสติก เพื่อการประเมินอย่างรวดเร็วถึงความสามารถในการรับแรงที่มากที่สุดของโครงสร้างที่ สามารถถูกใช้งานภายใต้ข้อกำหนดลิมิตสเตทได้อย่างปลอดภัย การดำเนินการของระเบียบวิธีออคทรีและโพลี กอนสเกลบาวดารีไฟในต์เอเลเมนต์สามารถสร้างแบบจำลองทางกลศาสตร์ที่ถูกต้องแบบอัตโนมัติสำหรับ โครงสร้างที่มีรูปร่างที่ซับซ้อน ดังนั้นประโยชน์ที่ได้รับจากชุดระเบียบการวิเคราะห์โครงสร้างที่ถูกพัฒนาขึ้นใน งานวิจัยนี้ ได้แก่ สเกลบาวดารีไฟในต์เอเลเมนต์ สมูทไฟในต์เอเลเมนต์ที่โหนด และ สมูทไฟในท์เอเลเมนต์ที่ ขอบ คือ ซอพแวร์คอมพิวเตอร์ที่สามารถวิเคราะห์และประเมินค่าสัดส่วนความปลอดภัยของระบบโครงสร้าง พื้นฐานของประเทศ เพื่อเป็นข้อมูลประกอบการติดสินใจของหน่วยงานผู้รับผิดชอบ ในการวางแผนบำรุงรักษา

The project proposes the development of an innovative technology for numerical simulation and the development of an invaluable numerical tool for the effective safety assessment of engineering structures. Whilst most of the available analysis and design techniques are likely to suffer from the needs to extensively explore in an evolutive fashion the complete behaviors of large-scaled 3D structures, the proposed method overcomes the burden by extending scopes of classical plastic analysis to capture directly the maximum load capacity such that structure can safely sustain under limit states criteria. The implementation of an integrated octree and polyhedron scaled boundary finite element (SBFE) method will offer the automatic and accurate model construction of wide-class structures with complex geometries. The unified analysis (including SBFE, node-based smoothed finite element and edge-based smoothed finite element) frameworks therefore will advantageously provide the cost-effective and advanced computing software for the safety assessment (namely the computation of a familiar safety factor) of the strategic nation infrastructures under variable load regimes, and can be practically applied by engineers to decide whether the structure involved is safe or requires necessary maintenances.

คำหลัก : Structural Safety; Structural Optimization; Plasticity; Scaled Boundary Finite Element; Smoothed Finite Element

เนื้อหางานวิจัย

1. วัตถุประสงค์

Many structures in Thailand have passed or are approaching their design life. Most of them have deteriorated to various extents with time. The safe and cost-effective management of ageing structures is becoming an increasingly urgent issue, and appears to be critical to the Thai economy. The assessment of their safety and serviceability, considering the intrinsic and inevitable nonlinear properties and variable load regimes, is crucial in deciding on the necessity and type of rehabilitation, or the retirement of the structure. Moreover, the wide class of structures targeted, especially those with complex geometry (such as penetrations, curve boundary and cracks), is the commonplace and most popular type of structures in Thailand. Their safe and cost-effective design is an essential requirement.

The safety assessment of many important existing structures and design of the new ones rests on limit states criteria. This is typically carried out through a nonlinear elastoplastic analysis based on a step-by-step evolutive "marching" approach that follows the whole time history of loading. However, in a large number of practical engineering situations the use of "direct" or "simplified" methods which avoids a computationally expensive time-stepping analysis, represents a useful, competitive and an increasingly appealing alternative.

One important class of such methods is plastic (limit) analysis [Kamenjarzh (1996)]. The area has been vigorously researched. The distinctive feature of a classical limit analysis is the determination of the load factor (or more precisely in practice, its upper and/or lower bounds) at which a critical event occurs, namely, plastic collapse. Despite of its popularity and maturity, limit analysis as a mathematical programming problem has unfortunately not gained much interest from practitioners due to their nonfamiliarity with the appropriate model construction within an optimization setting. To overcome this limitation, a wide class of modulus variation procedures (see e.g. [Jones GL and Dhalla (1981); .Marriott (1988); Seshadri R and Fernando (1992)]) has been developed to determine the collapse load limit from iteratively performing familiar elastic stiffness analysis computations. One particular and appealing instance is the

so-called elastic compensation method (or ECM) coined in [Mackenzie and Boyle (1993); Hamilton, et. al. (1996)]. More specifically, the elastic analysis performed at each iteration involves systematic adjustment of elastic moduli of some discrete elements, where the associated stress resultants computed in the previous step are higher than some predefined thresholds. This procedure takes into account stress redistribution during the plasticity process. With fast-growing computer technologies, the development of state-of-the-art computing software will fruitfully assist engineers by providing the preliminary and key information on the maximum load capacity of a particular structure that can safely sustain, prior to any extensive detailed investigations are performed as to decide whether the maintenance program is required or the structure of which is safe and serviceable. It thus presents the cost-effective and quick safety assessment procedure as compared to other available methods that are often expensive with physical sampling and experiments in a full-facility laboratory.

Form the aforementioned statements, the primary aims of the present project are:

- i) The development of self-adaptive polygon/polyhedron scaled boundary finite element (SBFE) based mesh construction of 2D/3D structures with complex geometries.
- ii) The development of an iterative elastic SBFE based analysis procedure that closely approximates the maximum load capacity of perfectly-plastic structures with complex geometries at failure.
- iii) The development of three-node node-based smoothed finite element (NS-FE) method adopting the simplest low-order (linear) displacement field formulations, where the developed framework is not only insensitive to the arbitrarily distorted mesh configuration but also locking-free under an incompressibility condition
- iv) The development of the iterative elastic edge-smoothed finite element (ES-FE) method, which incorporates the state-of-the-art automatic adaptive (non-uniform) mesh construction as well as enables the smoothed C^0 -continuous recovery stress field using the stress recovery technique [Zienkiewicz and Taylor (2000)].

2. วิธีทดลอง

The computational methods performed for the safety assessment of 2D- and 3D-structures are developed within the three main finite element, called scaled boundary finite element (SBFE), node-based smoothed finite element (NS-FE) and edge-smoothed finite element (ES-FE), frameworks. These are illustrated as follows.

2.1 Scaled Boundary Finite Element Framework

Generic SBFE model and formulations

The formulations describe the generic SBFE discretization [Wolf and Son (2000); Song and Wolf (2000)] of structures in 2D (and 3D) spaces. The relations are based on the assumptions of geometric linearity and elastic material properties. Unlike boundary element methods, the SBFE approach provides a semi-analytical solution of the subdomain, whilst standard finite element technique for plasticity is directly applicable in SBFEs. The SBFE implementation for elastoplastic analyses is reported in [Ooi, et. al. (2014)], where the merits of flexibility of meshing and efficient treatment of cracks/notches are demonstrated.

For clarity of the following expressions, a generic polygon-type SBFE subdomain [Song and Wolf (1997, 2000); Wolf and Song (2000)] in Fig. 1 is considered, where a scaling center "O" is defined to be visible from all boundaries. Each boundary contains line elements (see Fig. 1a) for a 2D curvilinear (η, ξ) coordinate system and doubly-curved surface elements (Fig. 1b) in a 3D (η, ζ, ξ) coordinate system.

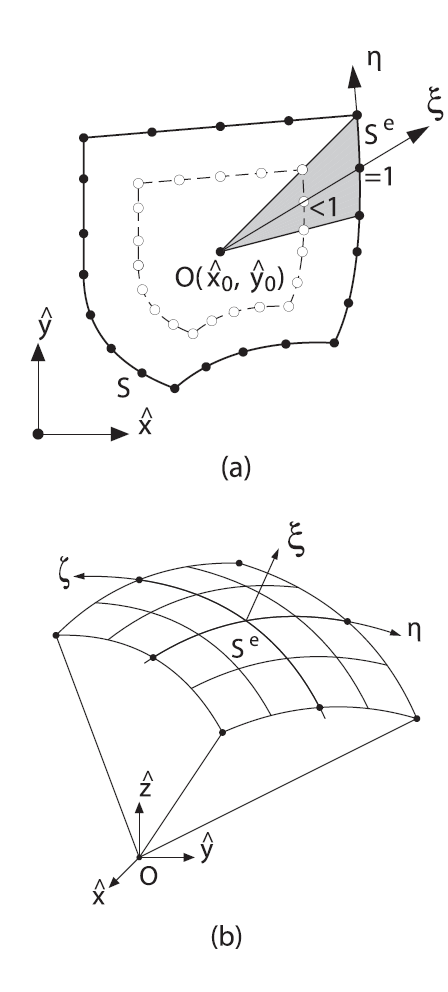


Figure 1. Generic SBFE subdomain (a) 2D case, (b) 3D case.

The geometry of the boundary along a circumferential direction is described using standard shape functions, namely $N(\eta)$ for $-1 \le \eta \le 1$ and $N(\eta,\zeta)$ for $-1 \le \eta \le 1$ and $-1 \le \zeta \le 1$ in 2D and 3D spaces, respectively. The dimensionless radial coordinate ξ describes the subdomain by scaling the boundary between the scaling centre (where $\xi=0$) and the boundary ($\xi=1$).

The local Cartesian (\hat{x}, \hat{y}) and $(\hat{x}, \hat{y}, \hat{z})$ coordinates can be expressed in terms of the curvilinear (η, ξ) and (η, ζ, ξ) coordinates by [24], viz.

in a 2D space:

$$\hat{x}(\xi,\eta) = \xi \ x(\eta) = \xi[N(\eta)]\{x\},\tag{1a}$$

$$\hat{y}(\xi, \eta) = \xi \ y(\eta) = \xi[N(\eta)]\{y\}$$
(1b)

and in a 3D space:

$$\hat{x}(\xi,\eta,\zeta) = \xi x(\eta,\zeta) = \xi[N(\eta,\zeta)]\{x\},\tag{2a}$$

$$\hat{y}(\xi, \eta, \zeta) = \xi y(\eta, \zeta) = \xi [N(\eta, \zeta)] \{y\}, \tag{2b}$$

$$\hat{z}(\xi,\eta,\zeta) = \xi z(\eta,\zeta) = \xi[N(\eta,\zeta)]\{z\},\tag{2c}$$

where $\{x\}$, $\{y\}$ and $\{z\}$ are the nodal Cartesian coordinates.

For a generic SBFE subdomain, the displacement field adopts

in a 2D $^{(\eta,\xi)}$ coordinate system:

$$\{u(\xi,\eta)\} = [N^{u}(\eta)]\{u(\xi)\} = [N_{1}(\eta)[I], N_{2}(\eta)[I],...]\{u(\xi)\},$$
(3)

and in a 3D (η, ζ, ξ) coordinate system:

$$\{u(\xi,\eta,\zeta)\} = [N^{u}(\eta,\zeta)]\{u(\xi)\} = [N_{1}(\eta,\zeta)[I], N_{2}(\eta,\zeta)[I],...]\{u(\xi)\}$$
(4)

where $\begin{bmatrix}I\end{bmatrix}$ is an identity matrix of appropriate size.

The displacement functions $\{u(\xi)\}$ given in Eqs. (3) and (4) along the radial direction ξ can be obtained from

$$[E^{0}]\xi^{2}\{u(\xi)\}_{,\xi\xi} + ((s-1)[E^{0}] - [E^{1}] + [E^{1}]^{T})\xi\{u(\xi)\}_{,\xi} + ((s-2)[E^{1}]^{T} - [E^{2}])\{u(\xi)\} = 0$$
(5)

where s = 2 and 3 in 2D and 3D spaces, respectively. The assembly of key matrices [E'] for i = 0, 1 and 2 follows standard finite element procedures using the information of geometry and material properties involved [Song and Wolf (1997)].

The internal nodal forces along the radial direction are expressed as

$$\{q(\xi)\} = \xi^{s-2}([E^0]\xi\{u(\xi)\}_{,\xi} + [E^1]^T\{u(\xi)\})$$
(6)

Further, formulating the two Eqs. (5) and (6) as the first-order ordinary differential system with twice the number of unknowns results in

$$\xi \begin{cases}
\xi^{+0.5(s-2)} \{ u(\xi) \} \\
\xi^{-0.5(s-2)} \{ q(\xi) \} \end{cases}_{,\xi} = -[Z] \begin{cases}
\xi^{+0.5(s-2)} \{ u(\xi) \} \\
\xi^{-0.5(s-2)} \{ q(\xi) \} \end{cases},$$
(7)

where the Hamiltonian matrix [Z] is formed as

$$[Z] = \begin{bmatrix} [E^0]^{-1}[E^1]^{\mathrm{T}} - 0.5(s-2)[I] & -[E^0]^{-1} \\ -[E^2] + [E^1][E^0]^{-1}[E^1]^{\mathrm{T}} & -([E^1][E^0]^{-1} - 0.5(s-2)[I]) \end{bmatrix},$$
(8)

and the eigenvalue decomposition of $^{ extbf{ iny [Z]}}$ gives

$$[Z][\boldsymbol{\Phi}] = [\boldsymbol{\Phi}][\lambda] = \begin{bmatrix} [\boldsymbol{\Phi}_{u1}] & [\boldsymbol{\Phi}_{u2}] \\ [\boldsymbol{\Phi}_{q1}] & [\boldsymbol{\Phi}_{q2}] \end{bmatrix} \begin{bmatrix} [\boldsymbol{\lambda}_n] \\ [\boldsymbol{\lambda}_p] \end{bmatrix}_{,}$$
(9)

 $[\lambda_n]$ and $[\lambda_p]$ are eigenvalue matrices, whose real parts are negative and positive, respectively; $[\Phi_{u1}]$ and $[\Phi_{q1}]$ the eigenvectors of $[\lambda_n]$; and $[\Phi_{u2}]$ and $[\Phi_{q2}]$ the eigenvectors of $[\lambda_p]$.

The bounded domain is considered, where the associated eigenvalues retain only the negative real parts, leading to finite displacements at a scaling centre "O". Hence, substituting Eq. (9) into Eq. (7) provides the solutions of displacements and nodal internal forces as follows:

$$\{u(\xi)\} = \xi^{-0.5(s-2)} \Big[[\Phi_{u1}] \xi^{-[\lambda_n]} \{c\} \Big], \tag{10a}$$

$$\{q(\xi)\} = \xi^{+0.5(s-2)} \Big[[\Phi_{q1}] \xi^{-[\lambda_n]} \{c\} \Big]. \tag{10b}$$

The integration constants $\{c\}$ in Eqs. (10a) and (10b) are determined from the nodal displacements $\{u(\xi=1)\}$ on the boundary $(\xi=1)$ of the subdomain as

$$\{c\} = [\Phi_{u1}]^{-1} \{u(\xi = 1)\}$$
(11)

For each SBFE subdomain, the stresses $\{\sigma(\xi,\eta)\}$ and $\{\sigma(\xi,\eta,\zeta)\}$ are computed at an element level, and defined by

$$\{\sigma(\xi,\eta)\} = [D]([B^{1}(\eta)]\{u(\xi)\}_{,\xi} + [B^{2}(\eta)]\{u(\xi)\}/\xi),$$
(12a)

$$\{\sigma(\xi,\eta,\zeta)\} = [D]([B^{1}(\eta,\zeta)]\{u(\xi)\}_{,\xi} + [B^{2}(\eta,\zeta)]\{u(\xi)\}/\xi)$$
(12b)

where [D] is a material constitutive matrix, and $[B^1(\eta)]$, $[B^2(\eta)]$, $[B^1(\eta,\zeta)]$ and $[B^2(\eta,\zeta)]$) the strain and displacement expression terms [24]. Substituting Eq. (10a) into Eqs. (12a) and (12b) yields

$$\{\sigma(\xi,\eta)\} = \Psi_{\sigma}(\eta) \xi^{-[\lambda_n]-[I]}\{c\},\tag{13a}$$

$$\{\sigma(\xi,\eta,\zeta)\} = \Psi_{\sigma}(\eta,\zeta)\,\xi^{-[\lambda_n]-1.5[I]}\{c\},\tag{13b}$$

where

$$\Psi_{\sigma}(\eta) = [D](-[B^{1}(\eta)][\Phi_{u1}][\lambda_{n}] + [B^{2}(\eta)][\Phi_{u1}]), \tag{14a}$$

$$\Psi_{\sigma}(\eta,\zeta) = [D](-[B^{1}(\eta,\zeta)][\Phi_{u_{1}}][\lambda_{n}] - 1.5[I] + [B^{2}(\eta,\zeta)][\Phi_{u_{1}}]), \tag{14b}$$

define the stress modes associated with structures in 2D and 3D geometry systems, respectively.

Quadtree model construction of in-plane structural system

For the structural system that can be defined in a 2D space, the structural discrete model adopts the computationally advantageous quadtree mesh generation technique using polygon-shape SBFEs [Ooi, et. al. (2014, 2015)]. Such methodology provides the effective model construction of in-plane structures with complex geometries.

The algorithmic implementation of the quadtree SBFE model is summarized in Fig. 2, where $S_{\rm max}$ is the maximum allowed number of seed points in a cell, with S_b seed points on each boundary, and S_{roi} seed points around each region of interest, and $l_{\rm max}$ the maximum difference between the division levels of adjacent cells. In this scheme, the geometry information of the whole structural system is controlled by the signed distance function.

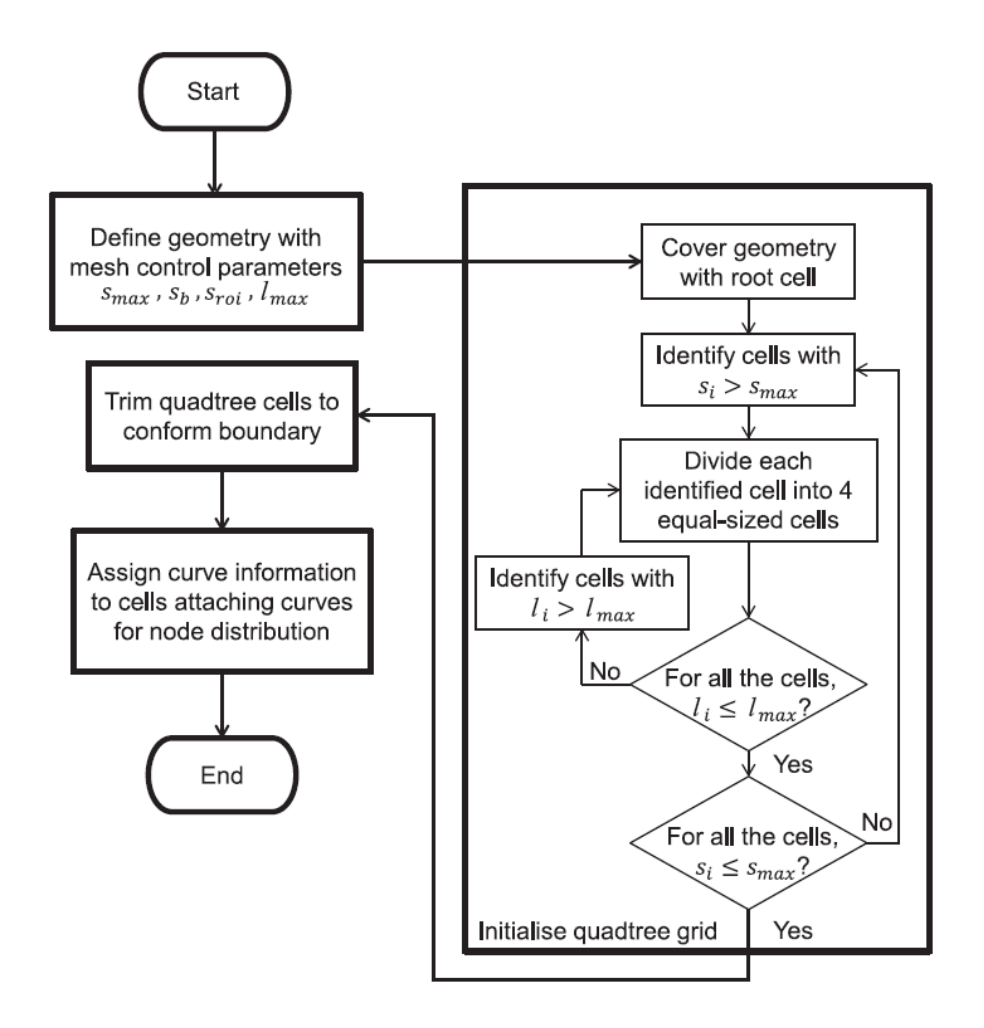


Figure 2. Flowchart for quadtree mesh generation procedures.

The function of a point $X \in \mathbb{R}^2$ within a SBFE subdomain Ω is graphically described in Fig. 3, and its mathematical description is given by

$$d_{\Omega}(x) = s_{\Omega}(x) \min_{y \in \partial \Omega} \|x - y\|, \tag{15}$$

where $\partial\Omega$ represents the boundary of the subdomain, $\|x-y\|$ is the Euclidean norm in R^2 with $y\in\partial\Omega$, and $s_\Omega(x)$ the sign function (namely -1 inside the subdomain or 1 otherwise). Boolean operations are employed to implement the complex geometry of the structure concerned [Talischi, et. al. (2012)].

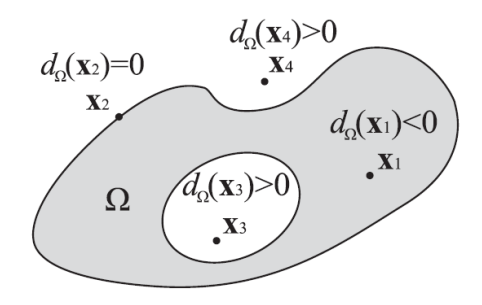


Figure 3. Signed distance function of a point inside the domain (X_1) , on the boundary (X_2) , and outside the domain (X_3) and (X_4) .

A series of seed points are predefined to control the local density and quality of the quadtree cells adopted in the boundary. The entire domain is initially covered by a single square, called root cell. The root cell is divided into four square cells, provided that the number of seed points S_i is larger than the maximum allowable limit of the corresponding cell, $S_{\rm max}$. This process is iteratively performed until the seed points of all cells is less than a pre-defined value.

At each iteration, the cell with high division level between the contiguous cells, namely $l_{\rm i}>l_{\rm max}$, is subdivided. The diagram in Fig. 4 illustrates the use of the recursive process used to obtain an initial grid in Fig. 4b of a square plate with penetration. In Fig. 4b, the initial quadtree mesh does not exactly conform to the boundary. Then, cells that intersect with the boundary are trimmed to form polygon shapes. The locations of vertices are defined by the direction and magnitude of the signed distance functions; the vertices on the boundary are assigned with solid square markers, whilst those inside the boundary with open square markers.

It is noted that weak shaped polygon cells, which contain much shorter edges as compared to the others, can be generated around the vertices close to the boundary. A threshold distance (e.g. 1/10 of the smallest cell edge attached to the vertex) determines whether those points are required to move to the boundary.

In Fig. 5, the implementation of the quadtree SBFE model over a circular penetrated plate is illustrated. In essence, Fig. 5a shows that coarse polygon meshes are first assigned on the

circular inner boundary. In Fig. 5b, the quadtree mesh refinement further enhances the SBFE discretization around the circular penetration using polygon-shape cells.

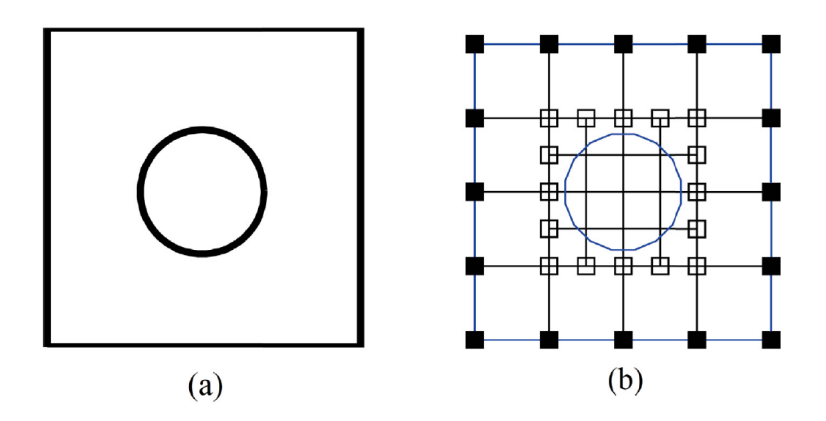


Figure 4. Square plate with circular hole (a) geometry, (b) initial quadtree grid mesh.

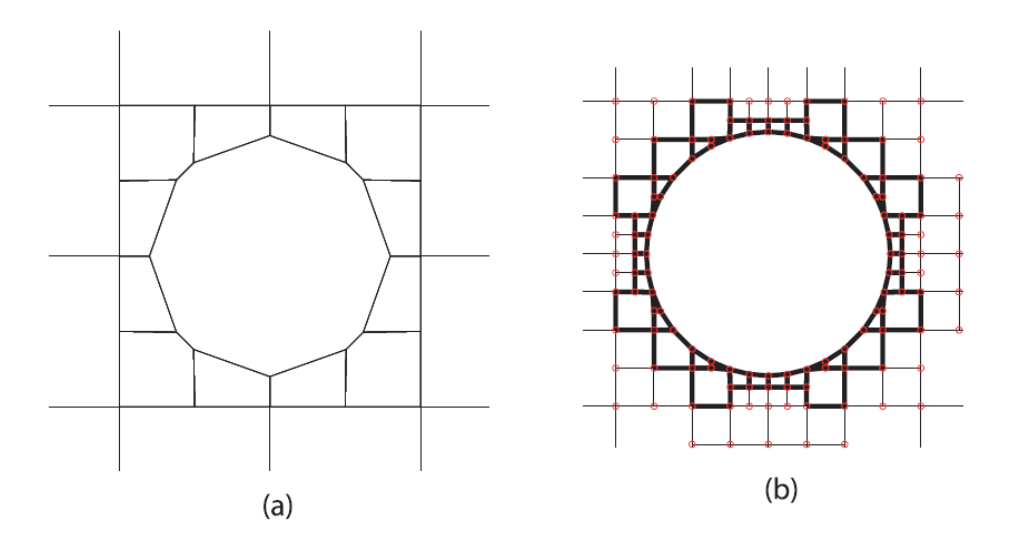


Figure 5. SBFE meshes around circular hole (a) standard polygon subdomains, (b) quadtree refinement.

Collapse load determination by iterative elastic SBFE analyses

The proposed approach performs an iterative series of elastic analyses for sufficiently ductile structures modelled within the effective polygon-shape SBFE and quadtree model construction framework [Ooi, et. al. (2015); Talishi, et. al. (2012)] to determine the maximum load capacity at plastic collapse. The method adopts the so-called modified elastic compensation algorithm [Yang, et. al. (2005); Chen, et. al. (2008)], and in effect represents an application of a lower-bound limit analysis.

The generic idea is simple in that a series of elastic SBFE analyses are iteratively processed. At the end of each iteration i, the computed statically admissible stress resultants are collected to calculate the corresponding load factor α' that complies with the plastic capacity of the material employed. At the beginning of the next iteration i+1, the stress resultants are collected to systematically adjust the elastic stiffnesses of some critical elements. This procedure is repeated until the predefined maximum number of iterations (imax) has been reached. The collapse load limit (α^{col}) is selected as the maximum load factor computed.

The structural system is suitably discretised using the quadtree polygon-shape SBFE model (namely n subdomains, d degrees of freedom and g numerical integration points) generation described in the previous section. The proposed numerical analysis determines the collapse load factor $\boldsymbol{\alpha}^{\text{col}}$ that can be safely sustained by the structure under monotonically applied forces $\boldsymbol{\alpha}^{\text{col}}$ that can be safely sustained by the structure under monotonically applied forces $\boldsymbol{\alpha}^{\text{col}}$, where $\{f\} \in \Re^d$ is a vector of basic forces. The approach enforces for each subdomain r the stress resultants $\boldsymbol{\sigma}^i_{r,j}$ at all integration points j=1 to g to comply with the failure conditions imposed by the specific material properties, such as von Mises (M) and Tresca (T) yield criteria, in 2D (or 3D) space as follows:

• 2D plane strain:

$$(\sigma_{r,j}^i)_M = \sqrt{\frac{3}{4} \{ (\sigma_x - \sigma_y)^2 + 4\tau_{xy}^2 \}}$$
(16a)

$$(\sigma_{r,j}^i)_T = \sqrt{(\sigma_x - \sigma_y)^2 + 4\tau_{xy}^2},$$
(16b)

• 2D plane stress:

$$(\sigma_{r,j}^i)_M = \sqrt{(\sigma_x - \sigma_y)^2 + \sigma_x \sigma_y + 3\tau_{xy}^2},$$
(17a)

$$(\sigma_{r,j}^i)_T = \max\left(|\sigma_1|, |\sigma_2|, |\sigma_1 - \sigma_2| \right), \tag{17b}$$

• 3D space:

$$(\sigma_{r,j}^{i})_{M} = \sqrt{\sigma_{x}^{2} + \sigma_{y}^{2} + \sigma_{z}^{2} - \sigma_{x}\sigma_{y} - \sigma_{x}\sigma_{z} - \sigma_{y}\sigma_{z} + 3(\tau_{xy}^{2} + \tau_{xz}^{2} + \tau_{yz}^{2})},$$
(18a)

$$(\sigma_{r,j}^i)_T = \max\left(\left|\sigma_1 - \sigma_2\right|, \left|\sigma_2 - \sigma_3\right|, \left|\sigma_3 - \sigma_1\right|\right), \tag{18b}$$

where $\{\sigma_x, \sigma_y, \sigma_z, \tau_{xy}, \tau_{xz}, \tau_{yz}\}$ and $\{\sigma_1, \sigma_2, \sigma_3\}$ are the standard sets of associated stress tensors and principle stresses, respectively. Different material laws can be enforced by simply redefining the stress resultants $\sigma_{r,j}^i$, such as ones given in Eqs. (16) to (18).

The algorithmic procedures iteratively adjust the elastic moduli of SBFE subdomains using the stress resultants at integration points computed in the previous analysis iteration. At the beginning of each iteration i+1 stress redistribution of some critical elements is implemented by systematically adjusting the stiffness properties (i.e. Young's modulus E_r^{i+1}) of the discrete elements. More explicitly, for the critical elements that contain the average stress resultants $\bar{\sigma}_r^i$ (where $\bar{\sigma}_r^i = \sum_{j=1}^g \sigma_{r,j}^i / g$) computed in the current iteration i greater than the nominal value $\bar{\sigma}_r^i$, their corresponding elastic stiffnesses are modified by

$$E_r^{i+1} = \begin{cases} E_r^i \frac{\overline{\sigma}^i}{\overline{\sigma}_r^i} & \text{if } \overline{\sigma}_r^i > \overline{\sigma}^i \\ E_r^i & \text{if } \overline{\sigma}_r^i \le \overline{\sigma}^i \end{cases}$$
(19)

where

$$\overline{\sigma}^{i} = \sigma_{\max}^{i} - \lambda \left(\sigma_{\max}^{i} - \sigma_{\min}^{i} \right) \tag{20}$$

where $^{\lambda}$ is a modification factor; and $^{\sigma^{i}_{\max}}$ and $^{\sigma^{i}_{\min}}$ the most maximum and minimum stress resultants developed in the whole structure, namely $^{\sigma^{i}_{\max}} = \max\left(\sigma^{i}_{r,j}\right)$ and $^{\sigma^{i}_{\min}} = \min\left(\sigma^{i}_{r,j}\right)$ for all elements r=1 to n and integration points j=1 to g, respectively.

One of the conditions underpinning the lower bound limit analysis theorem is the yield conformity over the whole structural system. Numerically, the plastic material properties are enforced solely at some predefined critical locations, namely integration points for each of the generic SBFEs. The proposed algorithm imposes such conditions by determining the associated (positive scalar) load factor of $\alpha^i = \sigma_o / \sigma_{max}^i$ that adjusts the magnitude of

stresses to lie within the maximum allowable yield stress σ_0 , where σ_{\max}^i is the largest maximum stress resultant of the whole structure. This ensures that the statically admissible stress resultants satisfy the allowable yield limit σ_0 . Therefore, for the total number (viz. *imax*) of iterative SBFE analyses the lower bound limit analysis determines the collapse load limit α^{col} of the structure by maximizing the load factor α^i , namely $\alpha^{col} = \max\{\alpha^i \mid i=1,\ldots,imax\}$.

The pseudo code summarizing key steps underlying the proposed iterative elastic SBFE analysis procedure is presented in the following:

Step 0: Initialization

- At iteration i=0, initialize: maximum number of iterations imax, elastic Young's modulus E^i_r , stress resultants $\sigma^i_{r,j}=0$ for all r=1 to n SBFE subdomains and j=1 to g integration points, yield limit σ_0 , Poisson's ratio v, $\overline{\sigma}^i=\sigma_0$, and $\lambda\in(0,0.5]$.
- Construct a quadtree polygon SBFE model, and assemble key vectors and matrices associated with the structure.

Step A: Iterative SBFE analyses

• For i = 1 to imax

Update the Young's modulus E_r^i for all n SBFE subdomains using Eqs. (19) and (20).

Process the elastic SBFE analysis in Eqs. (10), (13) and (14).

Determine the stress resultants $\sigma_{r,j}^i$ using appropriate Eq. (16), (17) or (18), and σ_{\max}^i .

Calculate the load factor $\, \alpha^i = \sigma_{
m o} \, / \, \sigma_{
m max}^i \, . \,$

End.

Step B: Termination

• Determine the collapse load $\alpha^{\text{col}} = \max\{\alpha^i \mid i=1,...,imax\}$, and plot the associated stress distributions at failure.

2.2 Node-Based Finite Element Framework

Generic three-node NS-FE model and formulations

Without undue loss of accuracy, the structure considered is modelled using an in-plane three-node NS-FE framework [Liu, et. al. (2009)]. The generic NS-FEs are depicted in Fig. 6, where the structure is discretized into N_n nodes, N_m members, N_d degrees of freedom and N_s smoothing domains (viz., a shaded area Ω_k^s for $\forall k \in \{1,\ldots,N_s\}$). Each discrete member is subdivided into three equally quadrilateral-shaped subdomains encompassed by its centroid (an opentriangle point), three-node vertices and mid-points on the element boundaries. The node-based smoothing domain Ω_k^s collects all subdomains enveloping the k-th common node (e.g., the smoothing node K involves six subdomains, namely KSRQ, KQPO, KONM, KMLJ, KJIH and KHGS lying within the six primal three-node elements KED, KDC, KCB, KBA, KAF and KFE, respectively). It is clear that the total number of smoothing domains N_s is identical to the number of nodes N_n , and the whole structural domain can be defined by $\Omega \equiv \bigcup_{k=1}^{N_s} \Omega_k^s$.

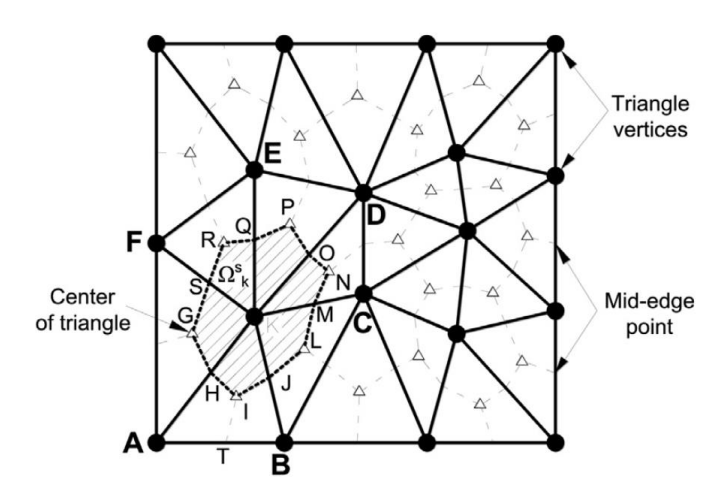


Figure 6. Generic three-node NS-FE model with smoothing (shaded) domains.

Underpinning the NS-FE, the strains are smoothed over all associated smoothing domains Ω_k^s using a weight-averaged strain field. The smoothed strain field ϵ_k of a generic domain Ω_k^s is expressed by

$$\mathbf{\varepsilon}_{k} = \int_{\Omega_{k}^{s}} \tilde{\mathbf{\varepsilon}}(x, y) W(x, y) d\Omega = \int_{\Omega_{k}^{s}} \begin{bmatrix} \partial / \partial x & 0 \\ 0 & \partial / \partial y \\ \partial / \partial y & \partial / \partial x \end{bmatrix} \mathbf{u}(x, y) W(x, y) d\Omega$$
(21)

where $\tilde{\mathbf{\epsilon}}(x,y)$ is a compatible strain field underlying standard three-node (viz., linear displacement field) finite element method, $W(x,y) \ge 0$ a Heaviside-type weight smoothing function:

$$W(x,y) = \begin{cases} 1/A_k^s, & (x,y) \in \Omega_k^s \\ 0, & (x,y) \notin \Omega_k^s, \int_{\Omega_k^s} W(x,y)d\Omega = 1, \end{cases}$$
(22)

 $A_k^s = \int_{\Omega_k^s} d\Omega$ collects the areas within a node-based smoothing domain Ω_k^s . For instance, in Fig. 1 the area of a smoothing-node K reads $A_k^s = \sum_{m=1}^6 (A_m/3)$, where A_m is the area of m-th primal element associated with individual subdomain enclosing the node.

The smoothed strain field is determined by Green's divergence theorem, and substituting Eq. (22) into Eq. (21) yields:

$$\mathbf{\varepsilon}_{k} = \frac{1}{A_{k}^{s}} \int_{\Omega_{k}^{s}} \tilde{\mathbf{\varepsilon}}(x, y) d\Omega = \frac{1}{A_{k}^{s}} \int_{\Gamma_{k}^{s}} \mathbf{L}_{n}(x, y) \mathbf{u}(x, y) d\Gamma, \ \mathbf{L}_{n}(x, y) = \begin{bmatrix} n_{x} & 0 \\ 0 & n_{y} \\ n_{y} & n_{x} \end{bmatrix}, \tag{23}$$

where $\mathbf{L}_n\left(x,y\right)$ is a matrix collecting outward normals (n_x,n_y) to the boundary Γ_k^s of Ω_k^s (e.g., in Fig. 6 a smoothing domain Ω_k^s of the node K containing twelve boundaries Γ_k^s along the segments SG, GH, HI, IJ, JL, LM, MN, NO, OP, PQ, QR and RS), and $\mathbf{u}(x,y)$ the displacement field with reference to global degrees of freedom. The smoothed strain vector $\mathbf{\epsilon}_k$ explicitly reads

$$\mathbf{\varepsilon}_k = \mathbf{B}_k \mathbf{d}_k = \sum_{n=1}^{N_n^k} \mathbf{B}_n \mathbf{d}_n \tag{24}$$

where N_n^k is the number of all nodes encompassing the smoothing domain Ω_k^s (e.g., in Fig. 6 $N_n^k = 6$ for the vertices A, B, C, D, E and F associated with the smoothing-node K), \mathbf{B}_n and \mathbf{d}_n are the smoothed strain-displacement matrix and the n-th nodal displacements.

The unassembled strain compatibility matrix \mathbf{B}_k and displacement vector \mathbf{d}_k of a generic smoothing domain Ω_k^s collect the submatrices \mathbf{B}_n and vectors \mathbf{d}_n corresponding to the enveloping nodes and degrees of freedom, respectively. An area-weighted average formulation [Liu, et. al. (2009)] then gives

$$\mathbf{B}_{k} = \frac{1}{A_{k}^{s}} \int_{\Gamma_{k}^{s}} \mathbf{L}_{n}(x, y) \mathbf{N}_{m}(x, y) d\Gamma = \frac{1}{A_{k}^{s}} \sum_{m=1}^{N_{m}^{k}} \frac{1}{3} \tilde{\mathbf{B}}_{m} A_{m}$$
(25)

where $\tilde{\mathbf{B}}_m$ is a standard compatible strain-displacement matrix of the m-th primal three-node finite element underpinning a smoothing subdomain Ω_k^s , and N_m^k the number of three-node elements sharing the common node k (see e.g., in Fig. 6 $N_m^k=6$ for the smoothing domain Ω_k^s consisting of six members KAB, KBC, KCD, KDE, KEF and KFA).

The smoothing Galerkin weak form [Liu, et. al. (2007)] reads

$$\sum_{k=1}^{N_s} A_k^s \delta \mathbf{\epsilon}_k^{\mathrm{T}} \mathbf{D}_k \mathbf{\epsilon}_k - \int_{\Omega} \delta \mathbf{u}^{\mathrm{T}} \mathbf{b} d\Omega - \int_{\Gamma} \delta \mathbf{u}^{\mathrm{T}} \mathbf{p} d\Gamma = 0$$
, (26)

where **b** are the body forces, **p** the tractions applied on the elemental boundary and \mathbf{D}_k the member elastic stiffness matrix. Therefore, the governing elastic stiffness equations of the structure modelled using the NS-FE framework [Liu, et. al. (2007, 2009)] can be familiarly written as

$$f = Kd, (27)$$

where as for standard finite element procedures the two vectors \mathbf{d} and \mathbf{f} collect the displacements and externally applied forces at all degrees of freedom, and the global stiffness matrix \mathbf{K} assembles the matrices \mathbf{K}_k of all $k \in \{1, \ldots, N_s\}$ smoothing domains Ω_k^s . The explicit expressions of the stiffness matrix \mathbf{K}_k for a generic node-based smoothing domain are

$$\mathbf{K}_{k} = A_{k}^{s} t \mathbf{B}_{k}^{\mathsf{T}} \mathbf{D}_{k} \mathbf{B}_{k} \tag{28}$$

where t is an element thickness, and the unassembled stiffness matrix \mathbf{D}_k is written in terms of elastic Young's modulus E_k associated with the smoothing domain Ω_k^s .

Automatic adaptive NS-FE seheme

This section proposes the computationally advantageous non-uniform adaptive mesh scheme within the sequential elastic NS-FE analysis framework. The adaptive NS-FE approach adopts the newest bisection procedure [Funken, et. al. (2011); Dörfler (1996)] that automatically refines the master element with plastic stress responses into two children elements. At the same time, the two children members with elastic stress responses are combined to reform one master member. This advantageously enables the optimal mesh construction over a series of iterative NS-FE analyses.

The Dörfler criterion [Dörfler (1996)] defines the set Ω_M of refining elements as well as the remaining set Ω_N for possible coarsening members (i.e., as is clear $\Omega_M \cup \Omega_N = \{1,\ldots,N_m\}$ and $\Omega_M \cap \Omega_N = \emptyset$). More explicitly, the members lying within the refining set (namely $m \in \Omega_M$) satisfy

$$\sum_{m \in \Omega_M} \eta_m > \theta \eta \tag{29}$$

$$\eta = \sum_{m=1}^{N_m} \eta_m \tag{30}$$

where η_m is a member error parameter, η global indicator and $\theta \in (0,1)$ mesh refinement threshold coefficient. It is clear that the parameter θ plays a vital role in controlling the total

number of critical refining elements (the members within Ω_M), where the low value of heta yields the small number of members in Ω_M and vice versa for the high value.

The newest bisection scheme [Rivara (1984)] subdivides a triangle-shaped element of the set Ω_M into two children counterparts by the line connecting a new midpoint on the longest edge and its opposite peak vertex (see Fig. 7). The midpoint is then set as a new peak node for the subsequent refinement.

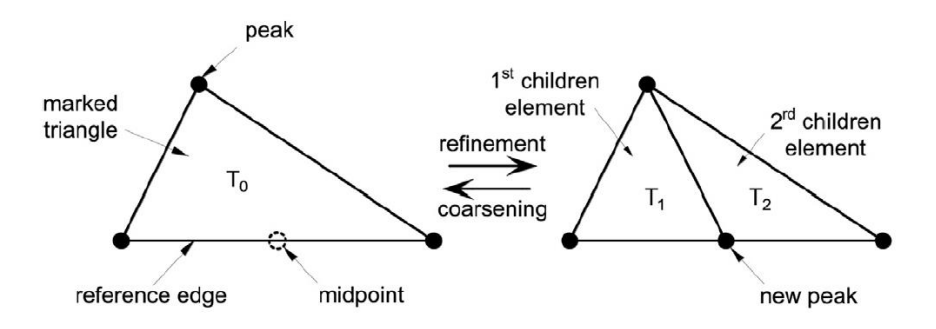


Figure 7. Newest bisection adaptive (refining and coarsening) mesh scheme.

The coarsening mesh construction [Chen and Zhang (2010)] presents a backward process to the newest bisection refinement. More explicitly, a pair of children elements in the set Ω_N previously refined are nested to form their master member. The bisection line connecting the peak vertex node and a midpoint is eliminated, and the midpoint is then removed from the longest edge. The two elements as consequence are fully merged. In the case of no midpoints presented for the elements in Ω_N only the refinement process is performed for those members in Ω_M .

The error function η_m in Eqs. (29) and (30) classifies whether the members are within the refining Ω_M or coarsening Ω_N set. The present work proposes the new error indicator based on the rate of modulus variations that characterize the equilibrium stress field at plastic failures, namely

$$\eta_m = E_m^{i=0} - E_m^{i=icol} \quad \forall m \in \{1, ..., N_m\}$$
(31)

where $E_m^{i=icol}$ is a modified m-th member modulus E_m^i at the i-th analysis iteration when $lpha^i=lpha_{col}$

The implementation of modulus variation-based error function in Eq. (31) explicitly determines the domains with inelastic localized stresses, which specially requires fine (non-uniform) mesh construction to capture plastic mechanisms. Those with acceptably low values of modulus variations are coarsened to reform their master elements. The resulting NS-FE model converges and depicts the yield line pattern of structures at failures.

Collapse load determination by iterative elastic NS-FE analyses

The proposed numerical method determines the maximum load capacity of an in-plane inelastic structure at plastic failures. Sufficient ductile materials and small deformations are assumed. The proposed scheme encoded within the NS-FE framework satisfies the statically admissible stress and yield conformity conditions underpinning the lower-bound limit analysis theorem. Whilst it preserves the simplicity in performing solely elastic analyses, the iterative NS-FE method (NS-FEM) can overcome the challenges in the presence of stress singularity and volumetric locking in an incompressibility.

The iterative elastic NS-FE analyses are based on the two-fold implementations. Firstly, the lower-bound limit analysis is performed by a modified version of elastic compensation method [Yang, et. al. (2005); Chen, et. al. (2008)] that generates the equilibrium stress fields through the process of modulus reductions in stress intensity areas. A number of successive elastic analyses within the reduced modulus procedure enable the stress redistribution from highly loaded elements to those with initially low stresses giving a series of different statically admissible stress fields. These equilibrium stress fields are enforced to conform with the yield limits by proportionally factoring the applied forces (viz., complying with the permissible maximum stresses throughout the whole structural domain), and establish the lower-bound theorem underpinning limit analysis. The accuracy and convergence of the lower-bound limit load solution depend on the robustness of discrete structural models at increasing mesh density. Secondly, the NS-FE method, as will be illustrated in the numerical algorithm, ensures

the volumetric locking-free behaviors in the presence of incompressibility conditions. Whilst the approach employs the low-order displacement formulations, it can efficiently provide the accurate elastic stress responses of structures and, as when incorporated within the modified elastic compensation method, the lower-bound collapse limit load results.

A modified version of elastic compensation method [Yang, et. al. (2005); Chen, et. al. (2008)], belonging to a wide class of modulus variation procedures [Mackenzie, et. al. (2000)], performs a series of successive elastic analysis solves with systematic adjustments of some elastic moduli associated with the critical elements developing intensive stresses. At each analysis iteration i, the algorithm explicitly determines the modified values of elastic moduli E_m^i of the m-th primal elements with the stress resultants $\sigma_{v,m}^{i-1}$ established in the previous iteration i-1 exceeding the predefined nominal limit σ_o^{i-1} . In essence, the modified modulus E_m^i of a generic m-th primal member reads:

$$E_{m}^{i} = \begin{cases} E_{m}^{i-1} \frac{\sigma_{o}^{i-1}}{\sigma_{v,m}^{i-1}} & \text{for } \sigma_{v,m}^{i-1} > \sigma_{o}^{i-1} \\ E_{m}^{i-1} & \text{for } \sigma_{v,m}^{i-1} \leq \sigma_{o}^{i-1} \end{cases}$$
(32)

$$\sigma_o^{i-1} = \sigma_{v,\text{max}}^{i-1} - \lambda \left(\sigma_{v,\text{max}}^{i-1} - \sigma_{v,\text{min}}^{i-1} \right)$$
(33)

$$\sigma_{v,\max}^{i-1} = \max(\sigma_{v,m}^{i-1} \mid \forall m \in \{1, ..., N_m\})$$

$$\sigma_{v,\min}^{i-1} = \min(\sigma_{v,m}^{i-1} \mid \forall m \in \{1, ..., N_m\})$$
(34)

where the nominal stress σ_o^{i-1} is defined as a function of the maximum $\sigma_{v,\max}^{i-1}$ and minimum $\sigma_{v,\min}^{i-1}$ stress resultants for all the elements $m \in \{1,\ldots,N_m\}$, and $\lambda \in (0,0.5]$ a modification factor. The critical elements requiring modulus E_m^i variations are classified in Eq. (32) by their corresponding stress resultants $\sigma_{v,m}^{i-1}$ being higher than the threshold σ_o^{i-1} , whereas those with smaller stress values remain unaltered.

The necessary plastic conformity conditions express the intrinsic material properties underpinning the structure through the following (nonpositive-sign constrained) yield functions $\phi(\sigma_{v,m}^i,\sigma_{c,m})$ for all N_m primal elements:

$$\phi(\sigma_{v,m}^i, \sigma_{c,m}) = \sigma_{v,m}^i - \sigma_{c,m} \le 0 \quad \text{for} \quad \forall m \in \{1, \dots, N_m\}$$
(35)

where $\sigma_{c,m}$ is a positive scalar defining material capacity of the m-th member. Such conditions permit direct scaling of the stress resultant response $\sigma_{v,m}^i$ by a maximum (positive-sign) load multiplier α^i that does not violate the plastic material constraints in Eq. (35):

$$\alpha^{i} = \min \left(\frac{\sigma_{c,m}}{\sigma_{v,m}^{i}} \mid \forall m \in \{1, \dots, N_{m}\} \right). \tag{36}$$

The lower-bound (static theorem) limit analysis then determines the collapse limit α_{col} of structure by maximizing the load multipliers α^i collected from all successive analysis iterations $i \in \{1, ..., imax\}$ of statically admissible stress field:

$$\alpha_{col} = \max \left(\alpha^i \mid \forall i \in \{1, ..., imax\} \right), \tag{37}$$

where imax is the targeted maximum number of iterations.

The proposed sequential elastic NS-FE analyses require solutions of the governing Eq. (27), which in effect involve a series of stiffness matrix \mathbf{K}_k constructions during the modulus variation procedures updated at an elementwise. The matrix \mathbf{K}_k is defined in Eq. (28) as a function of constitutive matrix \mathbf{D}_k and hence elastic Young's modulus E_k^i associated with the individual smoothing domain Ω_k^s . Each domain Ω_k^s (see e.g., Fig. 6) assembles all quadrilateral subdomains enveloping the k-th common node, and its modulus parameter E_k^i reads the smoothing product of those E_m^i determined in Eq. (32) for each of the relevant principal members. Therefore, the mathematical expressions of the modulus E_k^i collect and smooth

all modified elemental moduli E_m^i (for $\forall m \in \{1,...,N_m^k\}$) associated with the k-th smoothing node using the smoothing function W(x, y) in Eq. (22) by

$$E_k^i = \int_{\Omega_k^s} E_m^i(x, y) W(x, y) d\Omega = \frac{1}{A_k^s} \int_{\Omega_k^s} E_m^i(x, y) d\Omega$$
(38)

Adopting an area-weighted average function as for a smoothed strain field in Eq. (25) gives:

$$E_k^i = \frac{1}{A_k^s} \sum_{m=1}^{N_m^k} \frac{1}{3} E_m^i A_m \tag{39}$$

The determination of E_k^i in Eq. (39) enables at each analysis iteration i the fast construction of the governing stiffness matrices \mathbf{K}_k^i for $\forall k \in \{1, ..., N_s^k\}$ using some direct scaling factors,

namely
$$\frac{E_{k=1}^i}{E_{k=1}^{i=0}},\dots,\frac{E_{k=N_s}^i}{E_{k=N_s}^{i=0}}$$
, and hence the assembly of the global matrix **K** in Eq. (27).

The bi-level procedures, namely an inner-loop sequential modified modulus variation and an outer-loop automatic adaptive NS-FEM, determine the maximum load capacity α_{col} of structure and its corresponding plastic mechanisms. The pseudo-code summarizing the automatic adaptive iterative elastic NS-FE analysis method proposed is described as follows.

Step I: Initialization

- Parametric initialization: material properties (i.e., Young's moduli $E_m^{i=0}$, yield stresses $\sigma_{c,m}$ and Poisson's ratio v) and algorithmic parameters (modification factor $\lambda \in (0,0.5]$, mesh refinement threshold $\theta \in (0,1)$, maximum number of iterative NS-FE analyses imax, and maximum number of adaptive mesh constructions rmax).
- At the mesh construction r = 1, generate an initial structural three-node NS-FE model.
- Go to Step II.

Step II: Iterative elastic NS-FE analyses

- At the analysis iteration i=1, update the elastic moduli $E_m^{i=1}=E_m^{i=0}$ for all $m\in\{1,\ldots,N_m\}$ elements.
- For i = 1 to imax
 - Construct the unassembled stiffness matrices \mathbf{K}_k of the smoothing domains Ω_k^s for $\forall k \in \{1,...,N_s\}$ in Eq. (28), and the governing elastic NS-FE analysis Eq. (27).
 - Determine the smoothed strains $\mathbf{\epsilon}_k^i$ in Eq. (24) and hence stress resultants $\sigma_{v,m}^i$ associated with the primal members $m \in \{1,...,N_m\}$ by processing Eq. (27).
 - Calculate the maximum statically admissible load multiplier $lpha^i$ in Eq. (36).
 - Update for the next analysis iteration i+1 the modified moduli E_m^{i+1} for all $m \in \{1,\dots,N_m\}$ members in Eq. (32).

End

- Determine the collapse load limit α_{col}^r in Eq. (37).
- Go to Step III.

Step III: Automatic adaptive NS-FE model

- If r = rmax, terminate; else, update r = r + 1 and perform the adaptive NS-FE scheme.
- Compute the modulus variation-based error indicators η_m for $m \in \{1,...,N_m\}$ members in Eq. (31) and a global indicator η in Eq. (30).
- ullet Classify the individual members lying either in the refining Ω_M or coarsening Ω_N set using Eq. (29).
- ullet Reconstruct the NS-FE model by performing the newest bisection mesh refinement for the members in Ω_M and the coarsening process for a pair of children members in Ω_N

• Repeat Step II.

2.3 Edge-Smoothed Finite Element Framework

Generic ES-FEM model and formulations

Using the lowest-order element in standard FEM, the structure is discretized into N_d degrees of freedom, and N_m three-node elements consisting of N_n nodes and N_s edges. The ES-FEM [Liu, et al. (2009)] introduces at each element a center node that equally divides the triangle-shaped member into three parts. Thereafter, the smoothing domain Ω_k^s associated with the edge $k \in \{1, \ldots, N_s\}$ is constructed by combining the domains having the same edge. It connects two endpoints of the edge and the centroids of the adjacent elements as shown in Fig. 8. As a result, the number of smoothing domains Ω_k^s for $k \in \{1, \ldots, N_s\}$ is equal to the number of edges N_s .

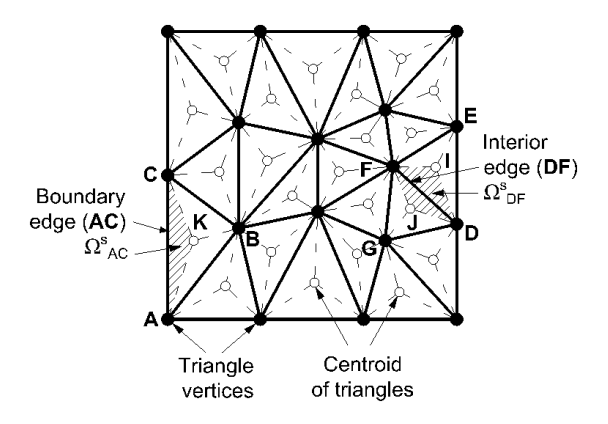


Figure 8. Generic three-node ES-FE model with smoothing (shaded) domains.

A smoothed strain $^{\mathbf{\epsilon}_k}$ within the smoothing domains $^{\mathbf{\Omega}_k^s}$ is given by

$$\mathbf{\varepsilon}_{k} \in \mathfrak{R}^{3} = \int_{\Omega_{k}^{s}} \tilde{\mathbf{\varepsilon}}(x, y) W(x, y) d\Omega \tag{40}$$

where $\tilde{\mathbf{\epsilon}}(x,y)$ is the compatible strain of a primal (three-node) element in FEM discretization

$$\tilde{\mathbf{\epsilon}} \in \mathbb{R}^3 = \begin{bmatrix} \partial / \partial x & 0 \\ 0 & \partial / \partial y \\ \partial / \partial y & \partial / \partial x \end{bmatrix} \begin{Bmatrix} u \\ v \end{Bmatrix} = \tilde{\mathbf{B}}_m \mathbf{d}_m$$
(41)

 $W(x, y) \ge 0$ is a Heaviside-type weight smoothing function satisfying the unity property

$$W(x,y) = \begin{cases} 1/A_k^s, & (x,y) \in \Omega_k^s \\ 0, & (x,y) \notin \Omega_k^s \text{ and } \int_{\Omega_k^s} W(x,y) d\Omega = 1 \end{cases}, \tag{42}$$

 $A_k^s = \int_{\Omega_k^s} d\Omega$ is the total area of an individual smoothing domain Ω_k^s , $\tilde{\mathbf{B}}_m \in \mathfrak{R}^{3 \times 6}$ and $\mathbf{d}_m \in \mathfrak{R}^6$ are respectively the standard strain-displacement matrix and nodal displacement vector associated with the primal element m encompassing the smoothing domain Ω_k^s .

By adopting the lowest-order element, the linear shape function gives a constant strain matrix $\tilde{\mathbf{B}}_m$ over an element. Therefore, the smoothed strain in Eq. (40) can be rewritten as

$$\mathbf{\varepsilon}_{k} = \begin{cases} \frac{1}{A_{k}^{s}} \left(\frac{A_{m}}{3} \tilde{\mathbf{B}}_{m} \mathbf{d}_{m} \right) & \text{involving one element } m \text{ for a boundary edge } k \\ \frac{1}{A_{k}^{s}} \sum_{m=1}^{2} \frac{A_{m}}{3} \tilde{\mathbf{B}}_{m} \mathbf{d}_{m} & \text{involving two elements } m \text{ for an interior edge } k \end{cases}$$

$$(43)$$

Green's divergence theorem is applied in Eq. (40), and the smoothed strain field then becomes

$$\mathbf{\varepsilon}_{k} = \frac{1}{A_{k}^{s}} \int_{\Omega_{k}^{s}} \tilde{\mathbf{\varepsilon}}(x, y) d\Omega = \frac{1}{A_{k}^{s}} \int_{\Gamma_{k}^{s}} \mathbf{L}_{n}(x, y) \mathbf{u}(x, y) d\Gamma, \quad \mathbf{L}_{n}(x, y) \in \Re^{3 \times 2} = \begin{bmatrix} n_{x} & 0 \\ 0 & n_{y} \\ n_{y} & n_{x} \end{bmatrix}, \tag{44}$$

where $\mathbf{L}_n(x,y)$ is a matrix collecting outward normal (n_x, n_y) acting on the boundary Γ_k^s of Ω_k^s , and $\mathbf{u}(x,y) \in \Re^2$ the displacement field. The smoothed strain vector $\mathbf{\epsilon}_k$ developed for the three-node ES-FE model then reads

$$\mathbf{\varepsilon}_{k} = \mathbf{B}_{k} \mathbf{d}_{k} = \begin{cases} \sum_{n=1}^{3} \mathbf{B}_{n} \mathbf{d}_{n} & \text{for } \Omega_{k}^{s} \text{ at a boundary edge } k \\ \sum_{n=1}^{4} \mathbf{B}_{n} \mathbf{d}_{n} & \text{for } \Omega_{k}^{s} \text{ at an interior edge } k \end{cases},$$

$$(45)$$

where the smoothed strain compatibility matrix \mathbf{B}_k and displacement vector \mathbf{d}_k collect the sub-matrices $\mathbf{B}_n \in \mathfrak{R}^{3 \times 2}$ and vectors $\mathbf{d}_n \in \mathfrak{R}^2$ of all vertex nodes n associated with the primal elements containing the domain Ω_k^s , respectively. As is clear, the domain Ω_k^s of a boundary edge k involves one primal member with three nodes at vertices (viz., $\mathbf{B}_k \in \mathfrak{R}^{3 \times 6}$ and $\mathbf{d}_k \in \mathfrak{R}^6$), whilst that of an interior edge k consists of two primal elements with four vertex nodes ($\mathbf{B}_k \in \mathfrak{R}^{3 \times 8}$ and $\mathbf{d}_k \in \mathfrak{R}^8$). An area-weighted average formulation [Liu and Trung (2016)] thus defines

$$\mathbf{B}_{k} = \frac{1}{A_{k}^{s}} \int_{\Gamma_{k}^{s}} \mathbf{L}_{n}(x, y) \mathbf{N}_{m}(x, y) d\Gamma = \begin{cases} \frac{1}{A_{k}^{s}} \left(\frac{A_{m}}{3} \tilde{\mathbf{B}}_{m}\right) & \text{for } \Omega_{k}^{s} \text{ at a boundary edge } k \\ \frac{1}{A_{k}^{s}} \sum_{m=1}^{2} \frac{A_{m}}{3} \tilde{\mathbf{B}}_{m} & \text{for } \Omega_{k}^{s} \text{ at an interior edge } k \end{cases}$$
(46)

where $\tilde{\mathbf{B}}_{j}$ is a compatible strain-displacement matrix extracted from the standard FEM.

The global elastic stiffness matrix $\mathbf{K} \in \mathfrak{R}^{N_d \times N_d}$ is assembled from the local matrices \mathbf{K}_k (where $\mathbf{K}_k \in \mathfrak{R}^{6 \times 6}$ for a boundary edge k, and $\mathbf{K}_k \in \mathfrak{R}^{8 \times 8}$ for an interior edge k) of all $k \in \{1, \ldots, N_s\}$ smoothing domains Ω_k^s that can be expressed by

$$\mathbf{K}_{k} = A_{k}^{s} t \mathbf{B}_{k}^{\mathsf{T}} \mathbf{D}_{k} \mathbf{B}_{k} \tag{47}$$

where $\mathbf{D}_k \in \mathfrak{R}^{3 \times 3}$ is a standard constitutive matrix written in terms of elastic Young's modulus E_k associated with a smoothing domain Ω_k^s . The elastic moduli E_k for all smoothing domains are calculated by the modulus smoothing approximation.

Recovery stress field

Within the strain-based ES-FEM framework, the smoothed C^0 -continuous stress field is estimated by the stress recovery technique [Zienkiewicz and Taylor (2000)]. In essense, the stress resultants $\sigma_{v,k}$ of all the relevant $N_{s,n}$ smoothing domains Ω_k^s are area-weight averaged around the node n, called first-order recovery nodal stress $\sigma_{v,n}$ [Nguyen-Xuan et al. (2013)]

$$\mathbf{\sigma}_{v,n} = \frac{1}{A_n^s} \sum_{k=1}^{N_{s,n}} \mathbf{\sigma}_{v,k} A_k^s, \tag{48}$$

where $A_n^s = \sum_{k=1}^{N_{s,n}} A_k^s$ is the total area of $N_{s,n}$ smoothing domains sharing the same node. The recovery stress field $\sigma_{v,r}(x,y)$ is approximated from the nodal stresses $\sigma_{v,n}$ of a generic three-node element m by

$$\mathbf{\sigma}_{v,r}(x,y) = \sum_{n=1}^{3} \mathbf{N}_n(x,y) \mathbf{\sigma}_{v,n}$$
(49)

where $\mathbf{N}_n(x,y)$ is a standard linear shape function.

The critical stress $\sigma_{v,m}$ of a generic three-node member $m \in \{1, \ldots, N_m\}$ reads the maximum $\sigma_{v,r}(x',y')$ of all three vertex nodes (x',y'). For example, in Fig. 8 for a triangle element DEF consisting of three vertices (x_D,y_D) at D, (x_E,y_E) at E and (x_F,y_F) at F, $\sigma_{v,m=DEF} = \max\{\sigma_{v,r}(x_D,y_D),\sigma_{v,r}(x_E,y_E),\sigma_{v,r}(x_F,y_F)\}$. The implementation of the recovery stress field $\sigma_{v,r}(x',y')$ advantageously ensures that the yield conformity is satisfied within an elementwise by enforcing the stress conditions solely at vertices (x',y') under the weak form of equilibrium conditions [Soh, et. al. (2001)].

Automatic adaptive ES-FE approach

The adaptive mesh scheme automatically determines the set $\Omega_{\rm M}$ of elements developing discontinuous distribution of inelastic stresses and required to refine the sizes. To keep a

number of elements as low as possible, the algorithm also defines the set Ω_N of members that contain relatively elastic stresses to be combined without undue loss of accuracy. It is clear that $\Omega_M \cap \Omega_N \in \varnothing$ and $\Omega_M \cup \Omega_N \in \{1, ..., N_m\}$.

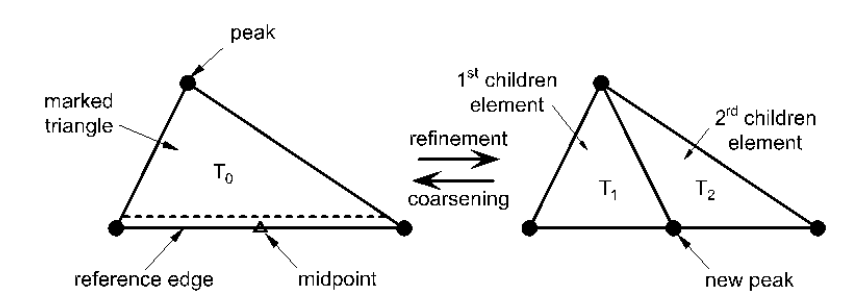


Figure 9. Adaptive mesh (refining and coarsening) construction.

The adaptive mesh refinement adopts the newest node bisection underpinning the longest-side bisection algorithm of triangles [Rivara (1984)]. As displayed in Fig. 9, a three-node element $m\in \Omega_M$ is divided into the new children triangles (i.e., connecting the peak to a midpoint of its longest edge). The midpoint is then set in a subsequent refinement as the peak point. Vice versa, the coarseness scheme combines the two adjacent sub-elements $m\in \Omega_N$ into a single element having now a larger size.

The set of elements $m \in \Omega_M$ complies with the well-known Dörfler condition [Dörfler (1996)] written in terms of the member error parameter η_m and global error indicator η :

$$\sum_{m \in \Omega_M} \eta_m \ge \theta \eta \tag{50}$$

$$\eta = \sum_{m=1}^{N_m} \eta_m \tag{51}$$

where $\theta \in (0,1)$ is a mesh refinement (threshold) coefficient. The specific error function is derived from the variations of member elastic moduli, where the specific member m enters plasticity with the reduction of stiffness modulus E_m^i . The error indicator η_m observes the difference between the elastic moduli $E_m^{i=0}$ of the primal members $m \in \{1,\ldots,N_m\}$ obtained

at the initial iteration i=0 and those E_m^{icol} associated with $\alpha^i=\alpha_{col}$, and can be mathematically expressed by

$$\eta_m = \left(E_m^0 - E_m^{icol}\right) \text{ for all } m \in \{1, ..., N_m\}$$
(52)

Collapse load determination by iterative elastic ES-FE analyses

A pseudo code describing the automatic adaptive iterative elastic ES-FE analysis procedures is summarized as follows.

Step I: Initialization

Initialize ES-FE model and parameters at i=0: material properties (i.e., elastic Young's moduli $E_m^{i=0}$, yield stresses $\sigma_{c,m}$ and Poisson's ratio v), threshold adaptive $\theta \in (0,1)$, maximum number of iterative ES-FE analyses (inner-loop) i_{max} and maximum number of adaptive mesh schemes (outer-loop) r_{max} .

Update: i = i + 1 and $E_m^{i=1} = E_m^{i=0}$ for all m three-node elements. Go to Step II.

Step II: Automatic adaptive iterative elastic ES-FE analyses

For r = 1 to r_{max}

For i = 1 to i_{max}

- Perform the elastic ES-FE analysis by assembling the stiffness equations in Eq. (8).
- Construct the recovery stress field $\sigma_{v,r}^{l}$ in Eq. (49), and then determine the stress resultants $\sigma_{v,m}^{l}$ for all m $\in \{1,\ldots,N_m\}$ elements.
- Calculate the maximum load multiplier α^i in Eq. (37).
- Adjust the elastic Young's moduli E_m^l of the critical elements m in Eq. (32).
- Determine the elastic moduli E_k^i associated with all smoothing domains Ω_k^s using an area-weighted average Eq. (39) employed for the construction of ES-FE analysis equations run in the subsequent iteration i+1.

End.

- Determine the collapse load limit α_{col}^r in Eq. (36) and associated mechanisms.
- Compute the modulus compensation error indicators η_m and global indicator η in Eqs. (31) and (30), respectively.
- Determine the set Ω_M in Eq. (29) for refining (and the remaining set Ω_N for coarsening) the domains using the newest vertex bisection implementation.

End.

It is worth mentioning that the yield functions describing the intrinsic material behaviors are generally written as functions of stress resultants $\sigma^i_{v,k}$ (computed in the form of stress tensors $\sigma^i_k \in \Re^3 = \left\{\sigma_x, \sigma_y, \tau_{xy}\right\}$ associated with the smoothing domain Ω^s_k) and yield limit $\sigma_{c,m}$.

3. ผลการทดลอง

The applications of the developed computational methods in assessing the collapse load capacity of structures were presented. Their accuracy and efficiency in determining the maximum load carrying capacity of solid structures were validated and illustrated through the good comparisons with the results reported in literatures [Christiansen and Andersen (1999); Tin-Loi and Ngo (2003); Ciria et al. (2008); Nguyen-Xuan et al. (2016, 2017); Le (2016)]. One from a number of those, namely the collapse load determination of a double-edge notch specimen, was illustrated as follows.

3.1 Double-Edge Notch Specimen

A double-edge notch specimen in Fig. 10 under the total uniformly applied tensile force of 0.288 α was considered. The von Mises material with an elastic modulus of E=70 was employed. The reference value is $(\alpha^{col}/\sigma_o)^{ref}=4.6749$, where $\sigma_o=0.243$ [Tin-Loi and Ngo (2003)].

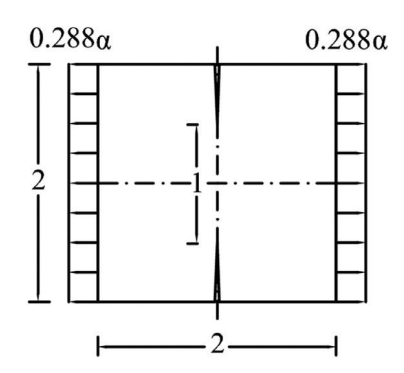


Figure 10. Double-edge notch specimen

3.2 Collapse load determination by iterative elastic SBFE analyses

Due to the symmetry of both geometric and applied loading configurations, a quarter of the tensile specimen was modelled using four-node bilinear SBFEs (containing 256 subdomains, 289 nodes, 578 degrees of freedom and 1024 Gauss's points) as shown in Fig. 11.

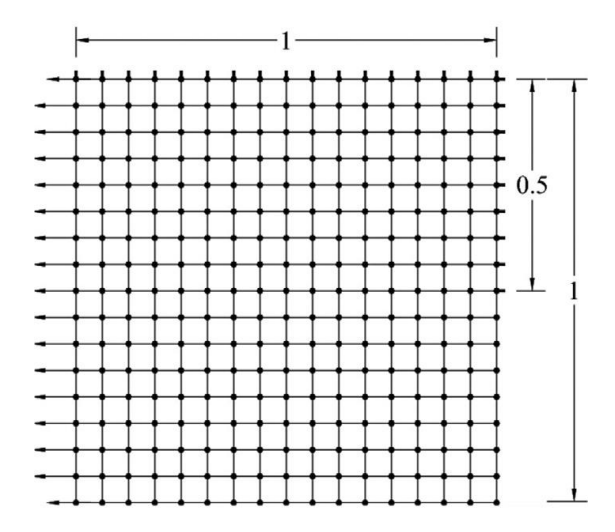


Figure 11. Schematic SBFE model.

A series of iterative elastic SBFE analyses were successfully performed. The values of load multiplier α' associated with each analysis iteration i are displayed in Fig. 12, which illustrates that the collapse load result of $\alpha'^{col}/\sigma_o = 5.0484$ is approached at i = 300. This represents some 7% higher value than the benchmark value. The corresponding stress distribution describing the collapse mechanism is depicted in Fig. 12b.

The tensile notch specimen was also employed to study the influences of plastic conformity locations as well as various algorithmic parameters λ on the accuracy of the computed

collapse load solution. More explicitly, when the locations of plastic conformity were defined at all nodes (ξ = 1 and η = ±1) in addition to standard integration points (ξ = 1 and η = 0) the value of $\alpha^{\rm col}/\sigma_{\rm o}$ = 5.0421 was computed by the proposed analysis approach. The same remark as in the previous example can be made. Plastic conformity located solely at the integration points is sufficient for the analysis to converge to the accurate collapse load solution.

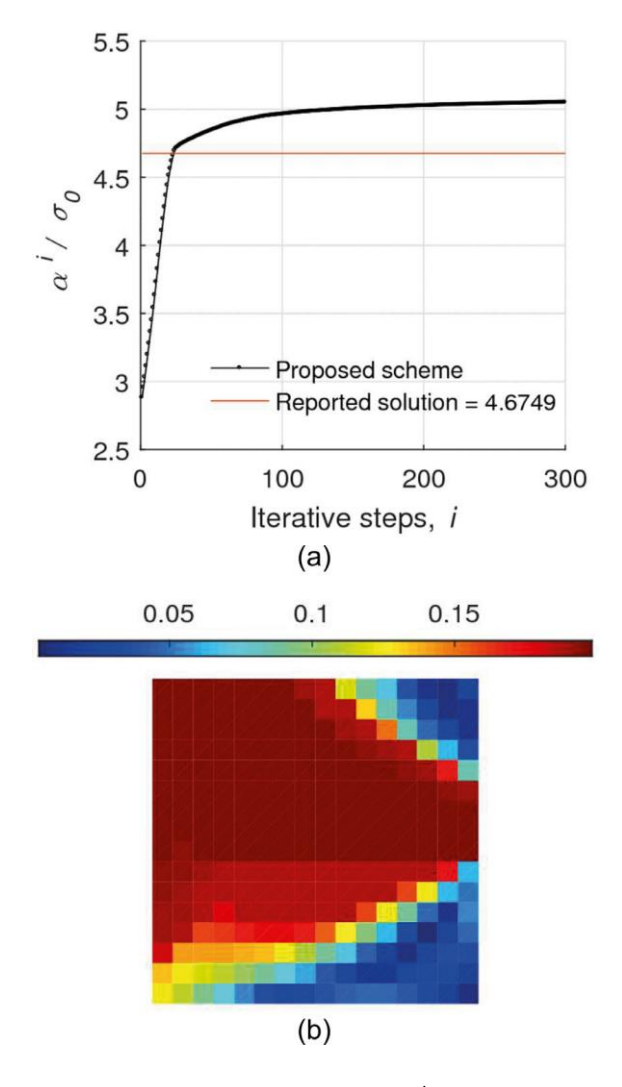


Figure 12. Iterative elastic SBFE analysis solutions (a) α^i/σ_o – i responses, (b) von Mises stress distribution at α^{col}/σ_o .

The responses between load multipliers $lpha^i$ and the associated number of iterations i are plotted in Fig. 13 for different values of λ lying within a range from 0.05 to 0.5. In essence, the analyses with the high value of λ (viz. a small value of $\bar{\sigma}^i$) admitted a large number of

critical SBFE subdomains r to adjust their elastic moduli E_r^i given in Eq. (19). The computation during the initial analysis iterations i attained the fast increment of an admissible load multiplier \mathbf{Q}^i , whilst the numerical instabilities (namely oscillation or even divergence of the \mathbf{Q}^i responses) were experienced in some cases after the certain analysis runs (e.g. $i \ge 9$ for $\lambda = 0.5$, and so on). On the other hand, the analysis with a small λ value provided a better chance to obtain good (numerically stable) convergence of the solutions giving a monotonic response of \mathbf{Q}^i . The diagram in Fig. 13 depicted with $\lambda = 0.05$ the progressive convergence of \mathbf{Q}^i to the actual collapse load solution \mathbf{Q}^{col} , but required a larger number of numerical iterations for the load limit to converge (i.e. as a less number of critical SBFE subdomains involved in the elastic modulus variation processes). In this study, the value of $\lambda = 0.05$ was found to yield good solution convergence for the numerical examples tested.

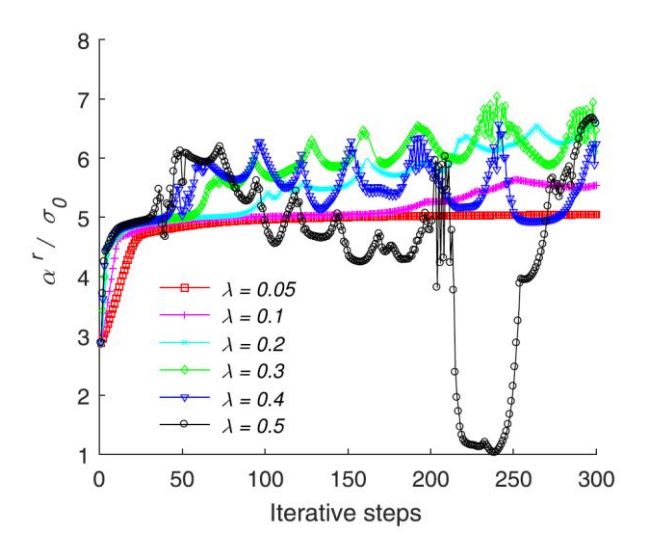


Figure 13. Iterative α^i/σ_o – i responses for various values of λ .

In addition, the iterative elastic SBFE analyses were performed for a series of SBFE models. Each involved a uniform structural discretization into four subdomains giving the numbers of SBFEs summarized in Table 1, where the computed collapse load solutions $\alpha^{\rm col}/\sigma_{\rm o}$ associated with each SBFE model are also collected. It is clearly evidenced that for sufficient numbers of SBFEs the collapse load limit converged to the lower-bound limit value. The analyses were also performed for standard finite elements with selective integration procedures [Hughes

(1980)]. The collapse load results obtained are reported in Table 1. This illustrates that the two SBFE and selective integration finite element analysis schemes computed accurate limit load solutions at a similar rate of mesh convergence.

Table 1. Double-edge notch specimen model and α^{col}/σ_o solutions for different structural discretization.

Stru	ctural disc	retization	SBFEs		Selective		
						integration FEs	
No. of	No. of	No. of	No. of				
subdomains	nodes	DOFs	Gauss's points	$lpha^{\!\scriptscriptstyle m col}\!/\sigma_{\!\scriptscriptstyle m o}$	%err	$lpha^{ m col}/\sigma_{\!\scriptscriptstyle m o}$	%err
			<u>'</u>				
16	25	50	64	6.1365	31.26	5.8807	25.79
64	81	162	256	5.4559	16.71	5.3004	13.38
256	289	578	1024	5.0484	7.99	4.9424	5.72
1024	1089	2178	4096	4.8055	2.79	4.7654	1.94
4096	4225	8450	16384	4.6733	-0.03	4.6543	- 0.44
16384	16641	33282	65536	4.6020	— 1.56	4.5885	— 1.85

3.3 Collapse load determination by iterative elastic NS-FE analyses

An upper-right quarter of the structure in view of its symmetric geometry and loading was modelled using three different (namely in Fig. 14 Case a crisscross-, Case b slash- and Case c distorted-) NS-FE models with initial 16, 32 and 32 basic elements, respectively. These three model cases were applied to illustrate the distinctive features of the iterative elastic NS-FEM in overcoming initial mesh dependency even for the distorted-type model construction.

In Case a, the crisscross-type model was processed to capture the collapse load $\alpha^{\rm col}$ by three different modelling approaches, including FEM, ES-FEM and the present NS-FEM. The $\alpha^{\rm col}$ solutions successfully computed from various uniformly refined NS-FE models (degrees of freedom, N_d) are plotted in Fig. 15 giving a direct comparison to those of FEM and ES-FEM. All $\alpha^{\rm col}$ responses converged to the lower-bound limit at sufficient fine structural discretization, whilst the NS-FEM performed slightly more superior than all others.

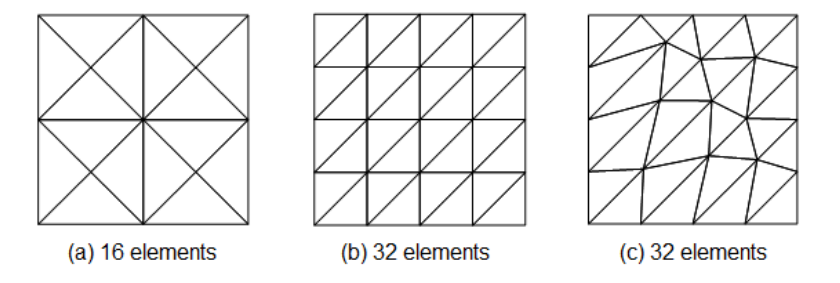


Figure 14. Various schematic NS-FE models of a quarter of double-edge notched specimen (a) crisscross-, (b) slash- and (c) distorted mesh pattern (δ = 0.5).

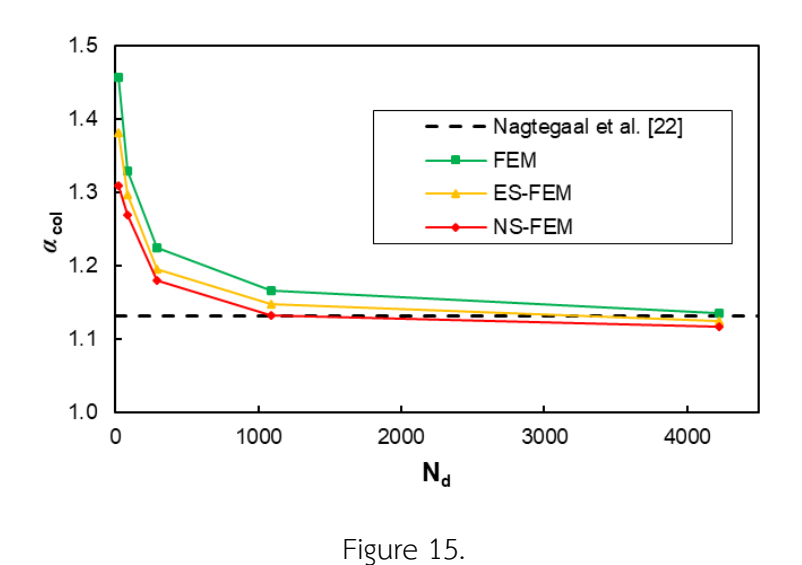


Figure 15. α col solutions for various crisscross-mesh models.

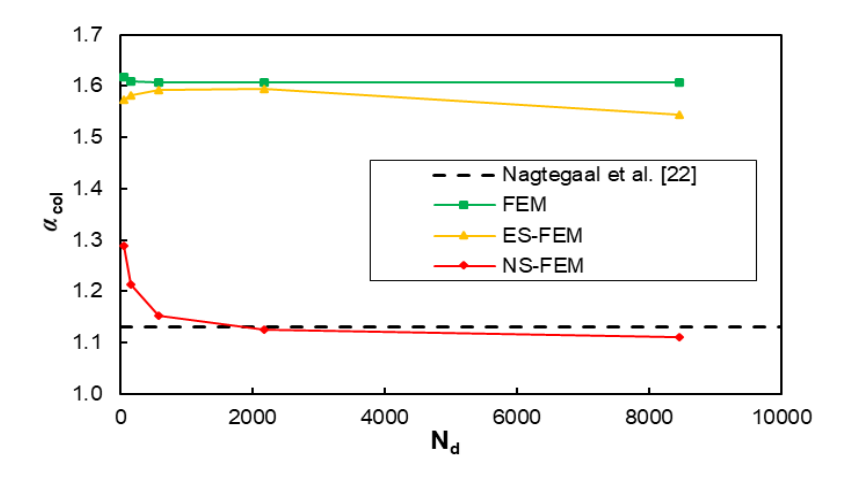


Figure 16. α col solutions for various slash-mesh models.

For the slash-mesh Case b model, both the FEM and ES-FEM failed to converge the lower-bound collapse load limit $\alpha^{\rm col}$ even for the large number of element refinements. The NS-FEM, on the other hand, captured the $\alpha^{\rm col}-N_d$ responses in Fig. 16 that converged quickly to the lower-bound limit. This, as illustrated previously by the high value of the ratio r_c , presents the good numerical performance of NS-FEM, which can overcome the volumetric locking phenomena in incompressible conditions underpinning the plane-strain structures [Liu, et. al. (2009); Mohapatra and Kumar (2019)]. The corresponding collapse mechanisms to the three NS-FE analysis results in Fig. 17 are mapped out.

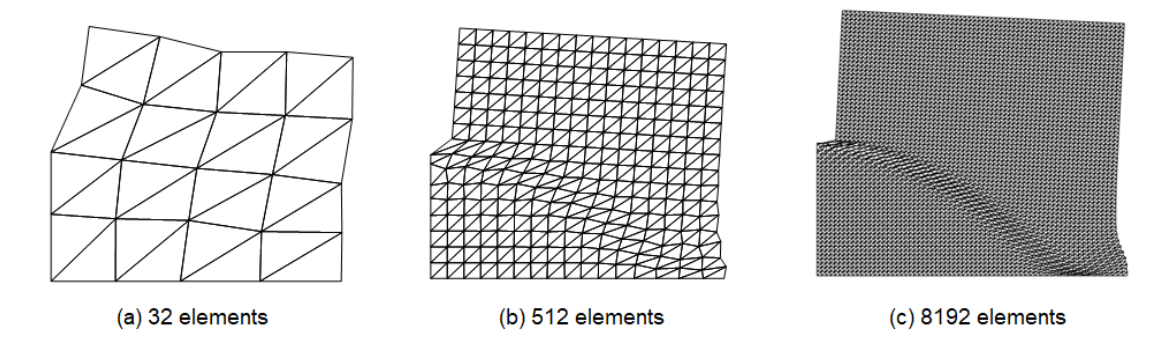


Figure 17. Deformations at plastic collapse for various uniform slash-mesh models.

The analyses of the distorted mesh Case c were performed. The coordinates (x', y') of the distorted model are varied by:

$$(x', y') = (x + r\delta.\Delta x, y + r\delta.\Delta y), \tag{25}$$

where $r \in [-1,1]$ is a random number, $\delta \in [0,0.5]$ an irregularity factor, Δx and Δy the initial edge lengths of a generic element along x- and y-directions, respectively. The $\alpha^{\rm col}$ responses computed by the proposed NS-FEM, having a highly-distorted shape with $\delta = 0.5$, were slightly above the solutions given by the uniformly refined slash counterpart (see Fig. 18). This evidenced the good performance of the sequential elastic NS-FEM that was not affected by the initial setup of mesh geometry even in the presence of strong mesh distortion in mapping the failure mechanisms [Ciria, et. al. (2008)].

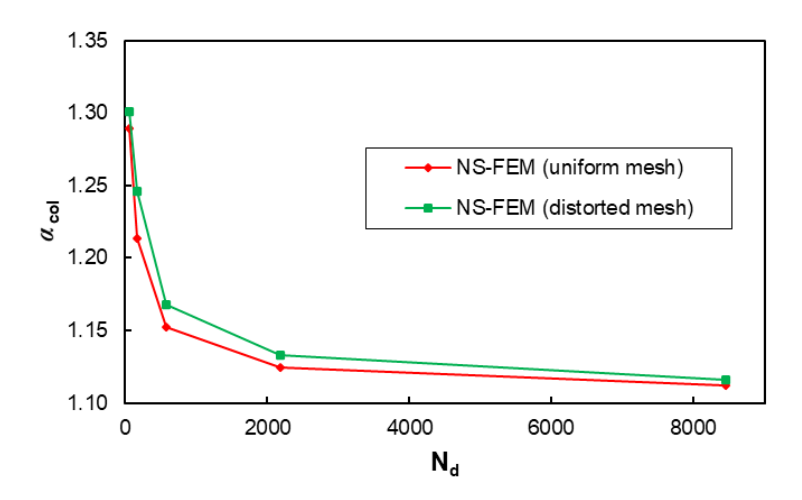


Figure 18. α col solutions for various distorted and slash-shaped NS-FE models.

The automatic adaptive mesh (newest bisection with a refining parameter of ϑ = 0.6) scheme was implemented directly to the slash-mesh model Case b. The $\alpha^{\rm col}$ solutions computed by the uniform and automatic (non-uniform) mesh refinements are reported in Table 2 that provides the direct comparisons between them. The analyses of both mesh refining schemes converged to the lower-bound limits. Moreover, the automatic adaptive (non-uniform) mesh models attended $\alpha^{\rm col}$ = 1.111 at much less computing resources (namely only N_m = 1370 and N_d = 1420), as compared to the uniform meshing technique (i.e., $\alpha^{\rm col}$ = 1.1117 when N_m = 8192 and N_d = 8450).

Table 2. α^{col} solutions of von Mises notched specimen ($\alpha^{\text{co,refl}}$ = 1.1316) by uniform and automatic adaptive NS-FEMs.

Uniform NS-FEM				Adaptive NS-FEM				
N _m	N _d	$lpha^{ m col}$	% error	-	N _m	N _d	$lpha^{ m col}$	% error
32	50	1.2892	+13.92		32	50	1.2892	+13.92
128	162	1.2136	+7.24		95	118	1.2112	+7.04
512	578	1.1521	+1.81		240	270	1.1472	+1.38
2048	2178	1.1245	-0.63		557	596	1.1198	-1.04
8192	8450	1.1117	-1.76		1370	1420	1.1110	-1.82

It is worthwhile noting that the iterative elastic NS-FE analysis approach established the lower-bound limit analysis theorems. Both the uniform and non-uniform adaptive NS-FE schemes complied with the statically admissible stress and yield conformity conditions, simultaneously. Whilst the exact collapse load solutions were not guaranteed, the proposed method, as listed in Table 2, ensured the close approximation and fast convergence (in the case of automatic mesh refinements) to the lower-bound limits of the structure. Moreover, as highlighted in the same Table 2, the values of $\alpha^{\rm col}$ in the early stage whilst lying on an upper bound side decreased quickly with the refinement of NS-FE models, depending on the appropriate mesh density over the failure zones. The variation of $\alpha^{\rm col}$, on the other hand, was insensitive to some further mesh refining schemes even in the critical areas, as when the collapse load was approaching some certain level toward the lower-bound limit.

A series of iterative NS-FE analysis iterations $i \in \{1, ..., imax\}$ with $\lambda = 0.05$ were performed for the non-uniform mesh model with 1370 elements, and the corresponding load multipliers α^i plotted in Fig. 19 evidenced the computational stability with monotonically increasing responses. Whilst the monotonic increases of the load multipliers α^i obtained by the proposed method enhanced the fast computation of the collapse load solution α^{col} in

general, it did not theoretically guarantee the numerical stability (slow solution convergence in some cases) over the modulus variation procedures. The sufficient number of elastic analysis iterations was necessary for the success of the analysis algorithm. From a number of examples tested, the preset maximum number of iterations, namely imax = 300, ensured the searches for the accurate α^{col} results.

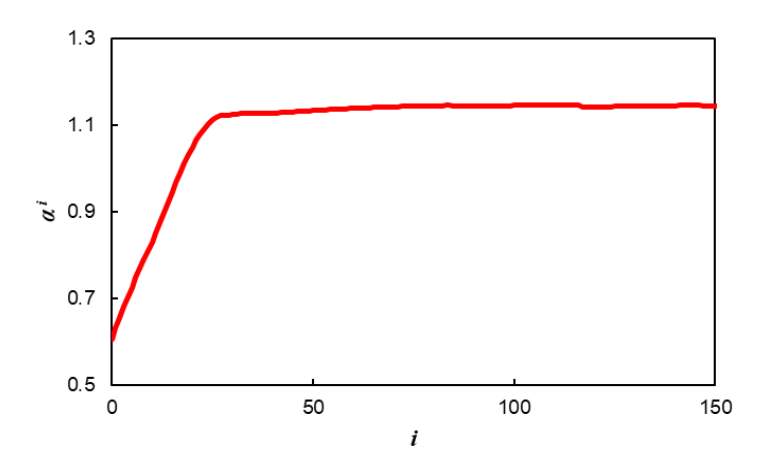


Figure 19. Monotonically incremental α i responses of a non-uniform NS-FE model with Nm = 1370.

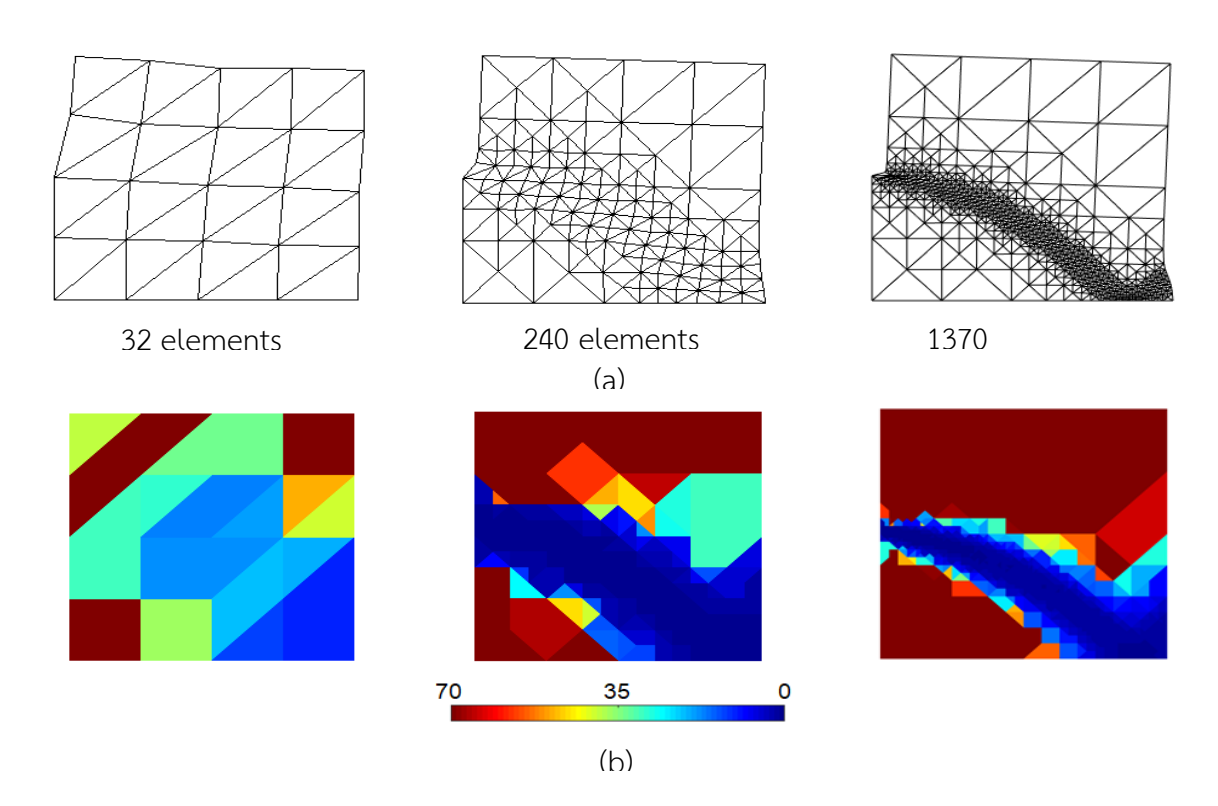


Figure 20. Collapse mechanisms for various non-uniform NS-FE models (a) deformations, (b) modified modulus distributions.

The resulting mesh layouts at some adaptive steps $r \in \{1, ..., rmax\}$ (consisting of 32, 240 and 1370 elements) are depicted in Fig. 20a with the associated modified modulus distributions in Fig. 20b, where the more density of elements was allocated to the areas having high modulus variation rates. They agree well with the yield line patterns and hence plastic mechanisms of the notched specimen under the ultimate forces [Nagtegaal, et. al. (1974); Füssl, et. al. (2008)].

Table 3. α^{col} solutions of von Mises notched specimen ($\alpha^{\text{col,ref}} = 1.1316$) by various analysis methods.

Approaches	$oldsymbol{lpha}^{ ext{col}}$	% error
Reference [Nagtegaal, et. al. (1974); Füssl, et. al. (2008)]	1.1316	n/a
Adaptive NS-FEM	1.1110	-1.82
Ciria et al. (2008)	1.1390	+0.65
Nguyen-Xuan et al. (2016)	1.1360	+0.39
Nguyen-Xuan et al. (2017)	1.1390	+0.65
Christiansen and Andersen (1999)	1.1358	+0.37
Le (2016)	1.1406	+0.21

The accuracy of the $\alpha^{\rm col}$ solutions performed by the present approach was validated by comparing with some available numerical methods summarized in Table 3, namely the second-order cone programming (e.g., kinematic [Nguyen-Xuan et al. (2016); Ciria et al. (2008); Nguyen-Xuan et al. (2017)] and static [Ciria et al. (2008); Le (2016)] limit analysis) approaches and mixed kinematic and static limit analysis [Christiansen and Andersen (1999)]. The percentage error (% *error*) draws the difference between the $\alpha^{\rm col}$ values of the analysis method and the ($\alpha^{\rm col}$)^{ref} reference in [Nagtegaal, et. al. (1974); Füssl, et. al. (2008)].

3.4 Collapse load determination by iterative elastic ES-FE analyses

A quarter (upper-right) of the specimen in Fig. 21 was modelled using 16 basic triangle elements and 26 degrees of freedom ($N_m = 16$; $N_d = 26$). The initial meshes were uniformly refined up to 8192 elements ($N_m = 8192$; $N_d = 8450$).

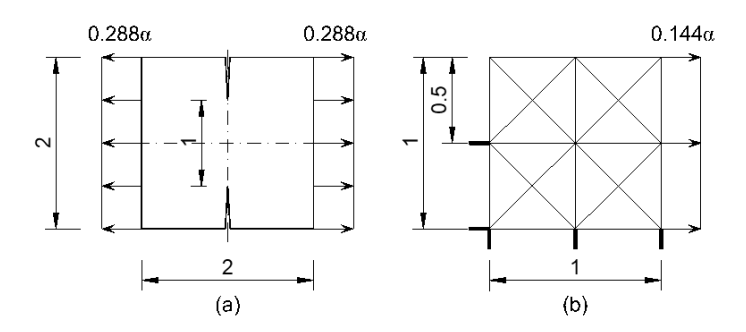


Figure 21. Double-edge notched specimen (a) geometry and loading, (b) schematic discrete model (Nm = 16), where solid lines indicate restrained boundary conditions.

The proposed iterative analyses adopted the self-adjusted modification factor λ taking into account of stress concentration developed close to the crack tip of the specimen. In the first instance, the ES-FEM with recovery stress field (RES-FEM) was performed to successfully compute the collapse load $\alpha^{\rm col}$ solution of the notched specimen with 8192 elements. The proportional load increment of α^i responses associated with the number of analysis iterations i was observed in Fig. 22, where the implementation of the dynamic modulus variation factor λ enhanced the fast computation of the collapse load solution, i.e., $\alpha^{\rm col}$ = 1.1244 being less than 1% difference to the reference value. The diagram showed the slowly converging yet oscillating (numerical instability) pattern of the resulting α^i variations, especially at the early analysis iterations i, for both the standard FEM and ES-FEM analysis frameworks. Their computed $\alpha^{\rm col}$ results required the more computing times to converge, as compared to that of the RES-FEM.

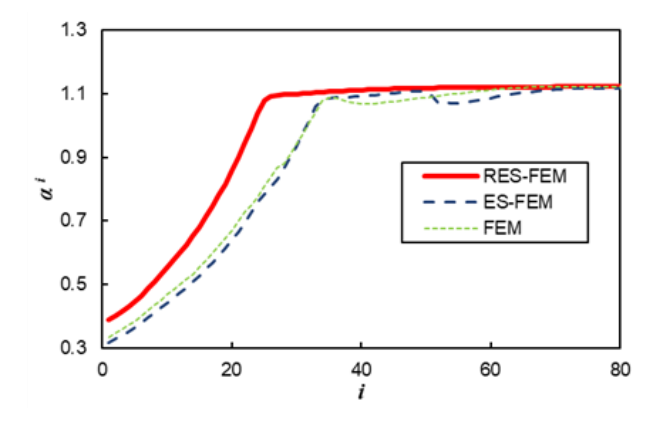


Figure 22. Double-edge notched specimen: load multiplier responses α i by RES-FEM, ES-FEM and FEM (Nm = 8192).

The second instance performed the automatic adaptive mesh algorithm within the RES-FEM. The results in Fig. 23 provided the direct comparison of the lower-bound limit convergence computed between the proposed adaptive mesh schemes and simple uniform mesh refinements. The α^{col} values for various structural discretization were reported in Table 4. More specifically, the adaptive mesh algorithm achieved the lower-bound collapse load of $\alpha^{\text{col}} = 1.1254$ (viz., 0.55% less than the reference value) with $N_m = 2952$. The uniform mesh refinement computed $\alpha^{\text{col}} = 1.1244$ at the more computing resources, namely $N_m = 8192$.

Table 4. Double-edge notched specimen: collapse load solutions $\pmb{\alpha}^{\text{col}}$ by various RES-FEM solves.

Uniform RES-FEM				Adaptive RES-FEM					
N _m	N _d	$lpha^{ m col}$	%error*	N _m	N _d	$lpha^{ m col}$	%error*	r	
16	26	1.4676	+29.70	16	26	1.4676	+29.70	1	
128	162	1.3162	+16.32	138	160	1.2686	+12.11	5	
512	578	1.2123	+7.13	363	392	1.1863	+4.83	7	
2048	2178	1.1470	+1.36	852	890	1.1460	+1.27	9	
8192	8450	1.1244	-0.64	2952	3012	1.1254	-0.55	12	

^{*} *%error* indicates the percentage error of α^{col} as compared to $\alpha^{col,ref} = 1.1316$.

Table 5. Double-edge notched specimen: collapse load solutions $\pmb{\alpha}$ col by various analysis methods.

Approach	N _m	$lpha^{ m col}$	%error
Reference [Nagtegaal et al. (1974)]	n/a	1.1316	n/a
Present (adaptive RES-FEM)	2952	1.1254	-0.55
Present (RES-FEM)	8192	1.1244	-0.64
Ciria et al. (2008)	5913	1.1390	+0.65
Christiansen and Andersen (1999)	n/a	1.1358	+0.37
Ciria et al. (2008)	5913	1.1320	+0.04
Nguyen-Xuan and Liu (2015)	3992	1.1360	+0.39
Le (2016)	2668	1.1406	+0.21

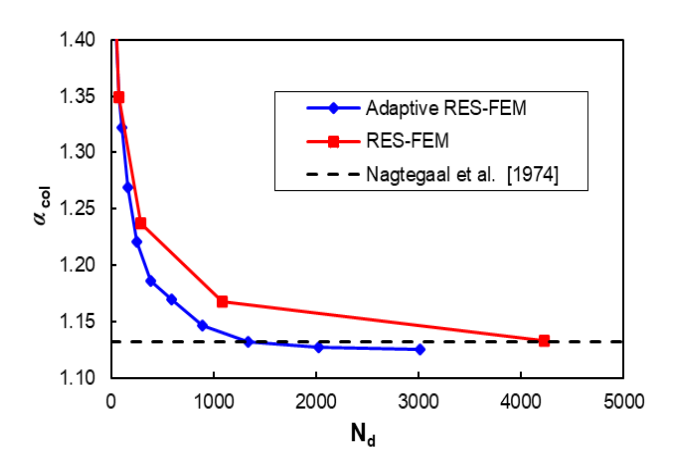


Figure 23. Double-edge notched specimen: collapse load solutions $\pmb{\alpha}$ col for various degrees of freedom Nd.

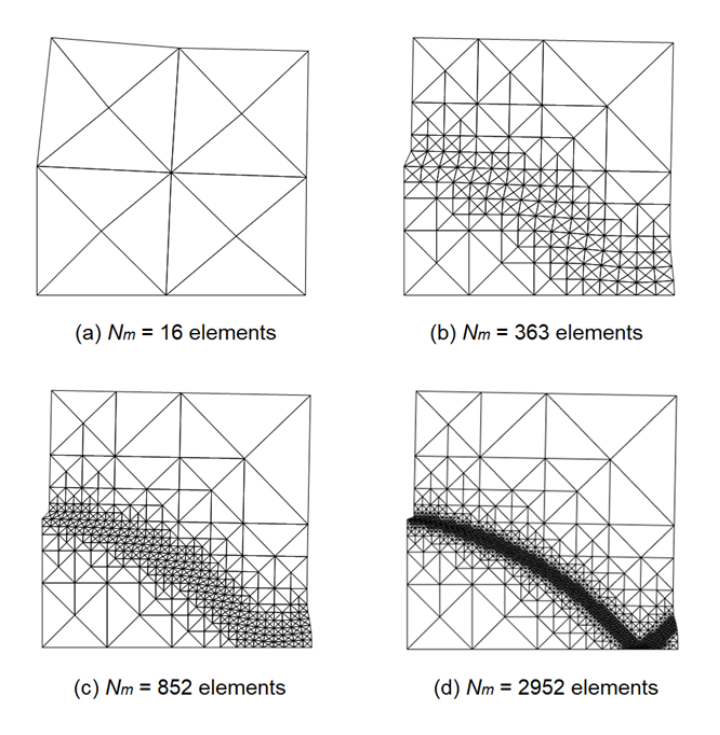


Figure 24. Double-edge notched specimen: progressive adaptive meshes of RES-FEM at α col.

The progressive adaptive meshes of the RES-FEM are displayed in Fig. 24 describing the failure lines of the double-notched specimen under applied forces. The more number of fine elements was defined over the area undergoing strong localized modulus variations and hence plasticity. This agrees very well with the collapse mechanisms reported in [Nguyen-Xuan et al. (2016)].

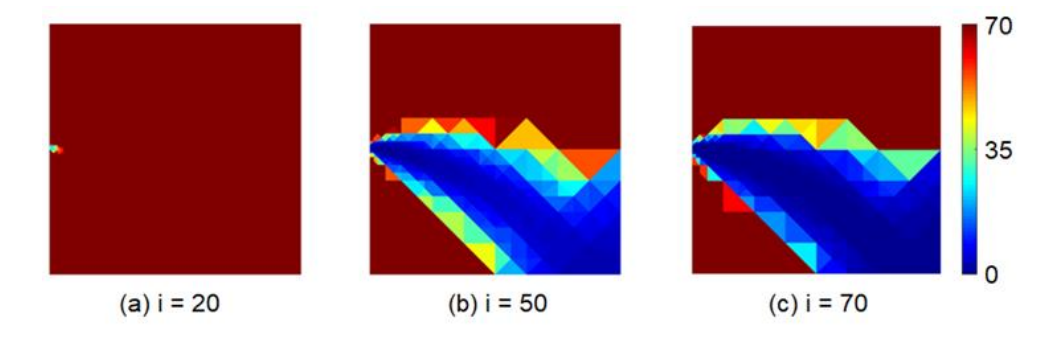


Figure 25. Double-edge notched specimen: modified modulus distributions by adaptive RES-FEM (Nm = 2952) at various iterations i.

In Table 5, the proposed analysis approach obtained the accurate collapse load solution as compared to some available literatures, including discrete duality method [Christiansen and Andersen (1999)], mesh adaptive schemes in lower and upper bound limit analyses [Ciria et

al. (2008)], ES-FEM with adaptive scaled-bubble functions [Nguyen-Xuan and Liu (2015)] and h-adaptive FEM with yield stress-based error indicators [Le (2016)]. The variations of modified moduli progressing over the localized failure area within the structure are plotted in Fig. 25 for some RES-FEM analysis iterations.

4. สรุปและวิจารณ์ผลการทดลอง

The project has developed the three robust numerical based frameworks that can be performed to assess the ultimate load carrying capacity of structures. First, the novel iterative elastic SBFE method has been proposed with the development of an effective structural discretization within a polygon-shape SBFE framework, in which a quadtree algorithm enables automated mesh construction of the structural system in a 2D space. The modified ECM processes a series of elastic stiffness analyses with a systematic modification of some elastic moduli to provide convergence to the collapse load limit solution.

Second, the iterative elastic NS-FE analyses incorporate an automatic adaptive mesh scheme to determine the collapse load limit of the plane-strain structures. The approach develops a modified version of an ECM run within the self-adaptive NS-FE framework. The newest bisection algorithm adopts a modulus variation-based error function such that the critical NS-FEs with localized inelastic stress responses are refined into the finer children elements and vice versa for the elastic stress elements being coarsened into the master counterparts.

Third, the iterative automatic adaptive ES-FE method performs a series of elastic recovery stress ES-FE analyses with the successive adjustment of elastic moduli to determine the maximum load capacity of inelastic structures. The new self-adjustable modification factor considers the influences of possible stress singularity developed leading to the monotonic increment of load multipliers during the modulus variation processes. The proposed approach importantly incorporates the first-order smoothed C0-continuous stress field, which enhances the sufficient and necessary static admissible stress and plastic material conditions conformed solely at the vertex nodes, and hence complies with the lower-bound limit analysis theorems.

Moreover, the automatic adaptive (non-uniform) mesh construction encoding the efficient newest bisection algorithm converges the lower-bound collapse load limit at modest computing resources. Underpinning the algorithm is the novel modulus compensation error function that effectively classifies the specific set of critical members requiring mesh refinements, and vice versa the elements lying outside this set are coarsened to maintain the total size of discrete model as minimum as possible.

A number of numerical examples (considering in-plane benchmarks, structures of complex geometry and 3D structures) have been successfully solved and hence illustrate the efficiency and robustness of the three developed numerical approaches. These include the inelastic structures with complex curve and/or vertex geometry subjected to the challenges involving stress singularity and volumetric locking in an incompressibility condition. Numerical stability can be achieved during the whole computing process, and the proposed schemes overcome the challenges related to stress singularity and volumetric locking phenomena under incompressibility conditions. The numerical experiments have shown there is no difficulty in obtaining accurate solutions as compared to available benchmarks. For all the numerical analysis frameworks developed, the solution converges to the lower-bound collapse load limit for the sufficiently fine model that is independent from the initial mesh (including the distorted pattern) setup. The final computed model advantageously depicts the yield line pattern (namely one containing dense meshes over the areas developing high stress intensity) associated with the collapse mechanisms of the structure considered.

A direct extension of the proposed analysis frameworks is the safety assessment of structures employing sustainable green constructional materials. This requires the investigation of basic properties of the materials specially mixed with some industry by-product wastes. For example, the project has further addressed the influences of recycled granite aggregate on the concrete properties. The use of granite industry waste as a mixing material of concrete reduces not only the natural aggregate consumption, but also the solid waste disposal

problems. Both the low- (20 MPa) and high- (50 MPa) strength concretes have been studied for various sand replacing proportions with granite particles (namely up to 50% by weight).

The future work therefore focuses on the development of the presented iterative elastic SBFE method that can directly assess the maximum load capacity of structures adopting the green concrete materials. This involves the solutions of difficult (ill-conditioning) mathematical programming problems involving strength-degrading (instability) constitutive models. The load carrying capacities of structures can also be assessed by performing the machine learning-based algorithms. The latter approach requires the sufficient (input and output) database modelled using the developed finite element frameworks.

เอกสารอ้างอิง

Chen, L., Liu, Y., Yang, P. and Cen, Z. (2008). Limit analysis of structures containing flaws based on a modified elastic compensation method. European Journal of Mechanics – A/Solids, 27: 195–209.

Chen, L. and Zhang, C. (2010). A coarsening algorithm on adaptive grids by newest vertex bisection and its applications. Journal of Computational Mathematics, 767-89.

Christiansen, E. and Andersen, K.D. (1999). Computation of collapse states with von Mises type yield condition. International Journal for Numerical Methods in Engineering, 46(8): 1185-202.

Ciria, H., Peraire, J. and Bonet, J. (2008). Mesh adaptive computation of upper and lower bounds in limit analysis. International Journal for Numerical Methods in Engineering, 75(8): 899-944.

Dörfler, W. (1996). A convergent adaptive algorithm for Poisson's equation. SIAM Journal on Numerical Analysis, 33(3): 1106-24.

Funken, S., Praetorius, D. and Wissgott, P. (2011). Efficient implementation of adaptive P1-FEM in Matlab. Computational Methods in Applied Mathematics, 11(4): 460-90.

Füssl, J., Lackner, R., Eberhardsteiner, J. and Mang, HA. (2008). Failure modes and effective strength of two-phase materials determined by means of numerical limit analysis. Acta Mechanica, 195(1-4): 185-202.

Hamilton, R., Mackenzie, D., Shi, J. and Boyle, J.T. (1996) Simplified lower bound limit analysis of pressurised cylinder/cylinder intersections using generalised yield criteria. International Journal of Pressure Vessels and Piping, 67: 219–26.

Hughes, T.J.R. (1980). Generalization of selective integration procedures to anisotropic and nonlinear media. International Journal for Numerical Methods in Engineering, 15: 1413-8.

Jones, G.L. and Dhalla, A.K. (1981). Classification of clamp induced stresses in thin walled pipe, In: Proceedings of the ASME Pressure Vessel and Piping Conference, Denver, Colorado, 81: 17–23.

Kamenjarzh, J.A. (1996). Limit Analysis of Solids and Structures. Boca Raton: CRC Press.

Le, C.V. (2016). Yield-stress based error indicator for adaptive quasi-static yield design of structures. Computers & Structures, 171: 1-8.

Liu, G.R., Dai, K.Y. and Nguyen, T.T. (2007). A smoothed finite element method for mechanics problems. Computational Mechanics, 39(6): 859-77.

Liu, G.R., Nguyen-Thoi, T. and Lam, K.Y. (2009). An edge-based smoothed finite element method (ES-FEM) for static, free and forced vibration analyses of solids. Journal of Sound and Vibration, 320: 1100–1130.

Liu, G.R., Nguyen-Thoi, T., Nguyen-Xuan, H. and Lam, K.Y. (2009). A node-based smoothed finite element method (NS-FEM) for upper bound solutions to solid mechanics problems. Computers & Structures, 87(1-2): 14-26.

Liu, G. R. and Trung, N. (2016). Smoothed Finite Element Methods, CRC Press.

Mackenzie, D. and Boyle, J.T. (1993). A method of estimating limit loads by iterative elastic analysis. I-simple examples. International Journal of Pressure Vessels and Piping, 53: 77–95.

Mackenzie, D. and Boyle, J.T. (2000). Hamilton R. The elastic compensation method for limit and shakedown analysis: a review. The Journal of Strain Analysis for Engineering Design, 35(3): 171-88.

Marriott, D.L. (1988). Evaluation of deformation or load control of stress under inelastic conditions using elastic finite element stress analysis, In: Proceedings of the ASME Pressure Vessel and Piping Conference, Pittsburgh, Pennsylvania, 136: 3–9.

Mohapatra, D. and Kumar, J. (2019). Smoothed finite element approach for kinematic limit analysis of cohesive frictional materials. European Journal of Mechanics-A/Solids, 76: 328-45.

Nagtegaal, J.C., Parks, D.M. and Rice, J.R. (1974). On numerically accurate finite element solutions in the fully plastic range. Computer Methods in Applied Mechanics and Engineering, 4: 153-77.

Nguyen-Xuan, H., Nguyen-Hoang, S., Rabczuk, T. and Hackl, K. (2017). A polytree-based adaptive approach to limit analysis of cracked structures. Computer Methods in Applied Mechanics and Engineering, 313: 1006-39.

Nguyen-Xuan, H., Wu, C.T. and Liu, G.R. (2016). An adaptive selective ES-FEM for plastic collapse analysis. European Journal of Mechanics-A/Solids, 58: 278-90.

Nguyen-Xuan, H., Liu, G.R., Bordas, S., Natarajan, S. and Rabczuk, T. (2013). An adaptive singular ES-FEM for mechanics problems with singular field of arbitrary order. Computer Methods in Applied Mechanics and Engineering, 253: 252–273.

Ooi, E.T., Song, C. and Tin-Loi, F. (2014). A scaled boundary polygon formulation for elastoplastic analyses. Computer Methods in Applied Mechanics and Engineering, 268: 905-37.

Ooi, E.T., Man, H., Natarajan, S. and Song, C. (2015). Adaptation of quadtree meshes in the scaled boundary finite element method for crack propagation modelling. Engineering Fracture Mechanics, 144: 101–17.

Rivara, M. C. (1984). Algorithms for refining triangular grids suitable for adaptive and multigrid techniques. International Journal for Numerical Methods in Engineering. 20(4): 745–756.

Seshadri, R., and Fernando, C.P.D. (1992). Limit loads of mechanical components and structures using the GLOSS R-node method. Journal of Pressure Vessel Technology, 1992;114:201-8.

Soh, C. K., Chan, T. K. and Yu, S. K. (2001). Numerical method for lower-bound solution of the rigid-plastic limit analysis problem. Journal of Engineering Mechanics, 127: 1075–1081.

Song, C. and Wolf, J.P. (1997). The scaled boundary finite-element method-alias consistent. Computer Methods in Applied Mechanics and Engineering, 147: 329–55.

Song, C. and Wolf, J.P. (2000). The scaled boundary finite-element method - a primer: solution procedures. Computers & Structures, 78: 211–25.

Talischi, C., Paulino, G.H., Pereira, A. and Menezes, I.F.M. (2012). PolyMesher: a general-purpose mesh generator for polygonal elements written in Matlab. Structural and Multidisciplinary Optimization, 45: 309–28.

Tin-Loi, F. and Ngo, N.S. (2003). Performance of the p-version finite element method for limit analysis. International Journal of Mechanical Sciences, 45: 1149–66.

Wolf, J.P. and Song, C. (2000). The scaled boundary finite-element method - a primer: derivations. Computers & Structures, 78: 191–210.

Yang, P., Liu, Y., Ohtake, Y., Yuan, H. and Cen, Z. (2005). Limit analysis based on a modified elastic compensation method for nozzle-to-cylinder junctions. International Journal of Pressure Vessels and Piping, 82(10): 770-6.

Zienkiewicz, O.C. and Taylor, R.L. (2000). The Finite Element Method, vol. 1, 5th edn. Butterworth Heinemann, Oxford.

ผลลัพธ์ที่ได้จากโครงการ

ผลงานตีพิมพ์ในวารสารวิชาการนานาชาติ

- 1. Mellati A, Tangaramvong S, Tin-Loi F and Song C (2020) An iterative elastic SBFE approach for collapse load analysis of inelastic structures. Applied Mathematical Modelling 81, 320-341.
- 2. Le VH, Tangaramvong S, Tran LV (2021) Sequential elastic adaptive NS-FE analyses for lower-bound limit load determination of plane-strain structures. International Journal of Mechanical Sciences 205, 106585.
- 3. Tangaramvong S, Nuaklong P, Khine MT and Jongvivatsakul P (2021) The influences of granite industry waste on concrete properties with different strength grades. Case Studies in Construction Materials, 15:e00669.
- 4. Le VH, Tangaramvong S, Tran LV (2022) Automatic Adaptive Recovery Stress ES-FEM for Lower-Bound Limit Load Analysis of Structures. International Journal of Computational Methods, 2141014:1-26.
- 5. Truong VH, Pham HA, Van TH, Tangaramvong S (2022) Evaluation of machine learning models for load-carrying capacity assessment of semi-rigid steel structures. Engineering Structures 273, 115001

การนำผลงานวิจัยไปใช้ประโยชน์

- เชิงวิชาการ (มีการพัฒนาการเรียนการสอน/สร้างนักวิจัยใหม่)

โครงการ "การประเมินความปลอดภัยของโครงสร้างโดยระเบียบวิธีพลาสติกสเกลบาวดารีไฟในต์เอเลเมนต์" ได้ถูกนำไปใช้ประโยชน์ในเชิงวิชาการ โดยสามารถสร้างองค์ความรู้ใหม่<u>และผลิตบุคลากร (ระดับปริญญาโท</u> จำนวน 2 คน และระดับปริญญาเอกจำนวน 1 คน) ทางด้านวิศวกรรมโครงสร้างที่มีความสามารถในการพัฒนา โปรแกรมคอมพิวเตอร์เพื่อการวิเคราะห์และประเมินความปลอดภัยของโครงสร้างและเครือข่ายสาธารณูปโภค ของประเทศ

อื่นๆ

- การเสนอผลงานในที่ประชุมวิชาการ
- 1. Tangaramvong S and Vu LH (2019) An efficient ES-FEM complementarity approach for post-collapse responses of concrete gravity dam (Proceedings, The Thirty-Second KKHTCNN Symposium on Civil Engineering, October 24-29, 2019, Daejeon, Korea).
- 2. Vu LH and Tangaramvong S (2019) The performance of ES-FEM with automatic triangle mesh adaptation in engineering mechanics applications (Proceedings, the 10th International Conference on Computational Methods, July 9-13, 2019, Singapore).
- 3. Vu LH and Tangaramvong S (2020) Automatic Adaptive ES-FE Approach for Limit Load Determination of Engineering Structures (Proceedings, the 11th International Conference on Computational Methods, August 9-12, 2020, Online).
- 4. Van TH, Le TM, Do B, Le-Duc T, Nguyen HD and Tangaramvong S (2020) A gaussian local search based particle swarm optimization for sizing and topology optimization of truss structure (Proceedings, The 3rd International Conference on Sustainability in Civil Engineering, November 26, 2020, Vietnam).